AD NUMBER

AD213227

NEW LIMITATION CHANGE

TO

Approved for public release, distribution unlimited

FROM

Distribution authorized to U.S. Gov't. agencies and their contractors; Administrative/Operational Use; 02 FEB 1959. Other requests shall be referred to US Office of Naval Research, Arlington, VA.

AUTHORITY

ONR ltr, DoDD 5200.20

213227

CREST RESEARCH LABORATORIES, INC.
a division of
MAGNA PRODUCTS, INCORPORATED
Santa Fe Springs, California

FINAL TECHNICAL REPORT

"MECHANISM OF CORROSION AND CORROSION INHIBITION OF STEEL IN WEAK ACID SOLUTION: DETERMINATION OF QUANTITATIVE LOCAL CELL POLARIZATION CURVES"

by

Willard R. Scott, Jr., Gilson H. Rohrback, and
Harold A. Parker-Jones

Contract No. Nonr 2113(00)

Office of Naval Research
Metallurgy Branch
Washington 25, D. C.

CREST RESEARCH LABORATORIES, INC.
a division of
MAGNA PRODUCTS, INCORPORATED
Santa Fe Springs, California

FINAL TECHNICAL REPORT

"MECHANISM OF CORROSION AND CORROSION INHIBITION OF STEEL IN WEAK ACID SOLUTIONS" DETERMINATION OF QUANTITATIVE LOCAL CELL POLARIZATION CURVES"

by

Willard R. Scott, Jr., Gilson H. Rohrback, and
Harold A. Parker-Jones

February 2, 1959

Contract No. Nonr 2113(00)

Office of Naval Research
Metallurgy Branch
Washington 25, D. C.

ABSTRACT

An apparatus and a procedure were developed for precise measurement of the mixed electrode potential, interface resistance, and interface capacitance of a corroding metal surface in the presence of polarizing current. The method was used, together with special instruments for measuring corrosion continuously, to obtain data from which quantitative local cell polarization diagrams could be constructed. Studies were made on mild steel corroding freely in oxygen-free salt water at pH 4 - 6, and on this electrode in the presence of several different types of corrosion inhibitors. Local cell polarization data for the inhibited surface were compared to those of the uninhibited surface, and certain conclusions were drawn regarding the mechanism by which inhibitors function.

ACKNOWLEDGEMENT

The support of this investigation by the Office of Naval Research is gratefully acknowledged.

TABLE OF CONTENTS

LIST OF TABLES

INTRODUCTION

The mechanism of corrosion of metals in contact with electrolytes has been established as an electrochemical one for many years. Since the time that the electrochemical theory was first proposed, the most widely used and revealing method for studying the electrical behavior of an electrode in solution has been the measurement of the electrode potential as a function of polarizing current. Polarization data resulting from such measurements are usually presented in the form of curves which may be analyzed in order to draw certain conclusions about the effect of variables.

The utility of these polarization curves in the study of corrosion inhibitors is based on the fact that under the proper conditions their slopes can be clues to interpretation of the manner in which inhibitors interact with the metal surface. At best, however, this type of polarization curve (i.e., potential vs. applied current) can give only an indirect indication of the true state of polarization on the surface. As pointed out by Mears and Brown (Ref. 1), the polarization characteristics of the local cells, rather than those of the surface as a whole, must be determined before a definitive picture of the metal-solution interface can be constructed.

Local cell polarization data, when available and properly presented, are invaluable for the elucidation of the mechanism of corrosion and corrosion inhibitor action. The rates of change of local anode and cathode potential with local cell current indicate which electrode process is controlling the corrosion rate, and changes in these rates of change may be attributed to adsorption of substances at the metal-solution interface. In addition, the local cell current corresponding to the point where the polarized

potential difference between anode and cathode areas becomes zero is equal to the limiting corrosion current, and this value is determined by the slopes of the potential functions for local anodes and cathodes. Thus, a knowledge of the local cell polarization curves permits one to account for observed corrosion behavior more or less completely.

Unfortunately, however, local cell polarization data are very difficult and time consuming to measure by methods which have been available to workers in this field in the past. Primarily for this reason the appearance of experimentally determined local cell polarization curves in the literature is rare, despite the unquestioned interpretative value of such data. That work which has been reported pertains to galvanic couples or other special configurations in which the anode area is distinct and separate from the cathode area, thus permitting certain simplifications of technique. To the knowledge of the authors of this report, no quantitative local cell polarization data have heretofore been reported for a corroding mixed electrode on which local anodes and cathodes are relatively small and are randomly distributed.

The main objective of the work described herein was to determine quantitative local cell data for one such mixed electrode. To facilitate the making of the required measurements, two new methods for measuring corrosion rates continuously were employed. These were (a) The Corroscmeter, an instrument system which measures loss of metal (anodic corrosion) directly without having to remove the specimen from the solution; and (b) a continuous hydrogen gas analyzer of high sensitivity, which permits following the rate of cathodic reduction of hydrogen ions in the solution. Without these two instruments it would not have been possible to obtain the data reported here.

Secondary objectives of the work were twofold: (a) to determine the effect of certain corrosion inhibitors on the local cell polarization curves; and (b) to derive from the data a further insight into the mechanism of corrosion and of corrosion inhibition. Analysis of the local cell curves obtained in the presence of corrosion inhibitors should show whether the observed effects are due to changes in open circuit potentials of local half-cells, to increased rate of change of EMF produced by local cell current, to increased interfacial resistances, or to some combination of these elements. This information in turn would allow more definite answers than have been heretofore available to such questions as: (1) Is the inhibitor adsorbed preferentially on local anodes or local cathodes; (2) Have the basic electrode processes been altered by the inhibitor, or have the reactive areas been reduced without being essentially changed; and (3) How has the relative distribution of corrosion current been changed.

The main body of this report is divided into four parts. Part 1 developes certain fundamental concepts necessary for a clear understanding of polarization data. This basic exposition was considered necessary because of the present ambiguity and lack of agreement which may be found in the existing literature on polarization phenomenon as it relates to the corrosion process. Part 2 describes the apparatus and methods used to obtain the data for construction of polarization diagrams. Part 3 presents the numerical results obtained, and Part 4 discusses these results. The discussion is devoted to pointing out the various emperical relationships that are evident from the data and to those interpretative comments that are supported by the limited amount of data available. A more exhaustive theoretical analysis would be beyond the scope of this work.

PART 1. THEORY AND BACKGROUND

1.1 It is generally recognized that the corrosion of iron (or steel) in acid solutions is an electrochemical process in which metal dissolves at relatively anodic points and hydrogen ions are reduced to hydrogen at relatively cathodic points on the metal surface. The anodic areas undoubtedly exhibit a variety of electrode potentials within a certain range of values, and the same may be said for cathode areas. To assist in the analysis of this distributed electrode activity, it is convenient to lump all anodes together and assign an average value of anodic potential, E_A, and of interfacial resistance, R_A. The same may be done for the cathodes giving a lumped cathodic potential E_C, and resistance R_C.(1)

1.2 For the hypothetical case in which no net current flows at the anodes, the potential difference across the metal-solution interface would be $E_A = (E_A)_c$ the so-called "open-circuit" potential of the anodes. If no net current were flowing at cathodes, the measured potential there would be $E_C = (E_C)_o$, the "open-circuit" potential of the cathodes. However, in all cases where corrosion occurs, some current does flow at anodes or cathodes or both. The respective potentials then are no longer equal to $(E_A)_o$ and $(E_C)_o$, and are said to be "polarized." The study of corrosion phenomenon so often involves measurement of polarized potentials that certain practical definitions of electrode potential which include IR drops have come into use. The

---

(1) Electrode potential symbols E_A and E_C will be used in this report to designate true EMF's, and are intended to include both activation energy effects and diffusion or concentration effects. Resistance symbols R_A and R_C will be used to designate that portion of any change of potential drop across an interface that varies linearly with current. According to the theory of electrode reactions, E_A and E_C, and to some extent R_A and R_C, are functions of the respective current densities.

following discussion is intended to distinguish between several of these as they relate to the present research.

1.2 If some net anodic current, i_A, flows (current flowing from local anodes into the solution), the average potential difference across the interface at anodic points will be

$$PD_A = E_A + i_A R_A \qquad \text{(Equation 1)}$$

Similarly, when a net cathodic current, i_C, flows (current from solution to the cathodes) the average potential difference across the interface at cathodic points will be

$$PD_C = E_C - i_C R_C \qquad \text{(Equation 2)}$$

Equations 1 and 2 constitute the definitions of the "polarized local anode potential" and the "polarized local cathode potential" that will be used in this report.

1.3 Individual anode and cathode potentials are somewhat hypothetical for steel undergoing corrosion in acid solution, inasmuch as local cell activity is distributed randomly over the surface. For this case, the nature of the electrode potential may be analyzed as follows: If it is assumed that the resistance through the electrolyte is negligible when compared to $R_A + R_C$ (a valid assumption when corrosion is uniform and local cells are close together), then the electrochemical behavior of the corroding metal surface may be represented by a simple equivalent circuit such as that shown in Figure 1. According to this picture, the local anode potential and local cathode potential are each polarized to the same value at the solution side of the electrochemical boundary layer (Point P, Figure 1). Thus, the potential difference between P and M, Figure 1, is given by

$$E_A + i_A R_A = E_C - i_C R_C = PD_P \qquad \text{(Equation 3)}$$

The potential difference expressed by Equation 3 is the so-called "mixed electrode potential," and is the potential difference that will be measured between the corroding metal and any reference half-cell located in the surrounding electrolyte, after the total potential difference has been corrected for any IR drops due to flow of current through the electrolyte as a whole. These remarks together with Equation 3, serve to define the "potential" of a mixed electrode for the purpose of this report.

1.4 Another concept of the mixed electrode potential appears in the literature, and should be clearly differentiated from the above. Some authors prefer to consider the potential to be a function only of the instantaneous values of E_A, R_A, E_C and R_C. The defining equation is

$$E_A + i_L R_A = E_C - i_L R_C = PD_L \qquad \text{(Equation 4)}$$

where

$$i_L = \frac{E_C - E_A}{R_A + R_C} \qquad \text{(Equation 5)}$$

PD_L will be referred to as the "reduced mixed potential."

1.5 The definitions of the two types of mixed electrode potentials given by Equations 3 and 4 are general, and are valid whether or not current is flowing to or from the corroding surface from an external source. When no such current is flowing, $i_A = i_C = i_L$, and Equations 3 and 4 become identical. In this case no problem arises from using the two concepts interchangeably. When current is flowing to or from a remote electrode, $i_A \neq i_C \neq i_L$, and so PD_P and PD_L diverge accordingly.

1.6 In the region where PD_p and PD_L are distinct, due to the effect of polarizing current at the interface, a simple relationship between the two potentials is provided by the circuit analogy discussed in Section 1.3. Referring to Figure 1, it may be shown (See Appendix A) that:

$$PD_p = PD_L \pm I_x R_f \qquad \text{(Equation 6)}$$

where I_x is the absolute value of the polarizing current, and R_f is the interface resistance in the path of I_x; thus

$$R_f = \frac{R_A \cdot R_C}{R_A + R_C} \cdot \qquad \text{(Equation 7)}$$

The plus sign in Equation 6 applies to anodic polarization; the minus sign to cathodic polarization.

1.7 The argument has been advanced (e.g., Ref. 2 and 3) that the potential designated as PD_L is a "pure" potential inasmuch as PD_L presumably contains no IR drop due to polarizing current. According to Equations 3, 4, and 6, each is a complex mixture of EMF's and IR drops, and neither should be referred to as "pure." Thus, the designation of PD_p and PD_L as "potentials" is less a matter of accuracy than of practical convenience.

1.8 Both PD_p and PD_L deserve attention in a study of local cell polarization and corrosion. The former is somewhat more useful in a practical sense, in that it is more sensitive to film resistance and corrosion current. The latter has somewhat more fundamental significance, reflecting only local half-cell EMF's and electrode resistances as they may be affected by adsorption and desorption at the interface.

1.9 The electrochemical behavior of a corroding metal-solution interface may be presented graphically by means of so-called polarization diagrams (Ref. 4 and 5). It is desired to distinguish between two different kinds

of diagrams which are often not clearly identified in the literature on corrosion. One shall be designated the "mixed potential polarization curve," and the other shall be designated the "local cell polarization diagram." The former is a plot of the mixed potential vs. the current impressed from an external source; the latter (local cell) diagram is a plot of local anode and local cathode half-cell potentials vs. local cell current. Both kinds of diagrams are instructive and both have been compiled for each system studied in the present work when the data was accessible.

1.10 Because so little quantitative local-cell polarization data has been reported, no uniform method of presenting the data has been developed. The method used in this report was chosen to display the data in a form that was considered to be most easily perceived and understood by those not entirely familiar with polarization phenomenon.

1.11 A hypothetical local cell polarization diagram is shown in Figure 2. The lines marked "Anodic" and "Cathodic" are the loci of the variations of local anodic and local cathodic polarized potentials, respectively. Thus, these two lines are described precisely by Equations 1 and 2, Section 1.2. In order to reconstruct such a diagram for an actual system, it is necessary to (a) vary the net anodic (or cathodic) currents in a known manner, and (b) measure the anodic (or cathodic) polarized potentials corresponding to known cell currents. According to the concept of local cell polarization adopted in this work (See Section 1.2) the currents referred to in (a) above are identical with i_A and i_C of Equations 1 and 2, and the potentials of (b) above are identical with PD_A and PD_C as defined by Equations 1 and 2.

1.12 These same two equations show that when $i_A = 0$, $PD_A = (E_A)_0$, the "open circuit" potential of the anodes; and when $i_C = 0$, $PD_C = (E_C)_0$, the "open circuit" potential of the cathodes. These two open circuit potentials are fundamental parameters in the analysis of polarization behavior, and thus the experimental set-up should be arranged to reduce i_A and i_C to zero if possible.

1.13 When the anodes are distinct and separated from the cathodes, as in some galvanic cells, it is possible to vary the cell current by means of an artificial resistance inserted in the metallic path. Anode and cathode potentials may be measured on separate and distinct areas, and the curves may then be drawn immediately from experimental data. Most local cell data reported in the literature has been obtained using such separable anodes and cathodes (Ref. 6, 7, 8, 9).

1.14 On the other hand, when anodes and cathodes are of microscopic size and are close together on a single corroding surface (such as they are during acid corrosion), the only practical way to vary i_A and i_C is to impress current from an external source. When the test surface is made cathodic with respect to the impressed current, i_A is reduced; when the test surface made anodic, i_C is reduced. (See Appendix A)

1.15 As specified in Section 1.11, local cell polarization curves consist of individual polarized potentials defined by Equations 1 and 2. Individual anode and cathode potentials cannot be distinguished on a mixed electrode, however, so they must be determined indirectly. Only the mixed potentials PD_p of Equation 3 can be measured opposite the mixed electrode. A comparison

of Equation 3 with Equations 1 and 2 shows that PD_p will equal PD_A when $0 \leq i_C \leq i_{corr.}$, where $i_{corr.}$ is the local cell current corresponding to the equilibrium corrosion rate. Similarly PD_p will equal PD_C when $0 \leq i_C \leq i_{corr.}$ Thus, the anodic branch of the diagram is determined by cathodic polarization, and the cathodic branch is determined by anodic polarization.

1.16 According to the above analysis, the two experimental variables which must be measured are (1) the net anodic or cathodic current flowing at the surface, and (2) the mixed potential PD_p. During cathodic polarization the net anodic current i_A is proportional to the rate of loss of metal. This rate data may be obtained by weight loss measurements, as has been reported (Ref. 1). However, weight loss methods were considered too cumbersome for the type of experiments planned. A continuous measure of anodic dissolution was highly desirable. At the time that this work was first proposed (1954) a method for following the corrosion rate of steel in acid solution continuously by means of hydrogen gas analysis had been developed (Ref. 10) and was being used in this laboratory. Hydrogen is generated by the cathodic reaction, and thus is a direct measure of anodic current only in the absence of impressed current. When impressed current is flowing, the anodic current (i_A) may be calculated from the values of the impressed current (I_x) and the total cathodic current (i_H) calculated from the rate of hydrogen evolution. The equation is:

$$i_A = i_H - I_x \qquad \text{(Equation 8)}$$

1.17 During anodic polarization, net cathodic current is measured directly by i_H, i.e., $i_C = i_H$, and thus the continuous hydrogen analysis technique could be used to measure local cell currents for both branches of the polarization diagram. This experimental approach was the one outlined in the original proposal for contract work.

1.18 Between the time that the proposal was submitted and the time work was begun, a second and more universally applicable method for measuring corrosion current continuously had been developed (Ref. 11). This method follows the change in electrical resistance of a metallic specimen, and thus gives a direct indication of the loss of metal from the surface. This data may be used to calculate the total anodic current, i_M. This data can also be used to calculate i_C resulting from anodic polarization by means of a relation similar to that of Equation 8, namely:

$$i_C = i_M - I_x \qquad \text{(Equation 9)}$$

The data so obtained could then be used to check that from hydrogen evolution. After certain minor problems of application had been worked out, the resistance method proved much simpler to use and more reliable than the hydrogen analysis method. Therefore, all anodic rate data were measured by the resistance technique rather than by use of Equation 8. Both methods were used at different times to measure the cathodic current.

1.19 The measurement of mixed potentials in the presence of impressed current presents certain experimental problems. The potential difference measured in any practical arrangement will include IR drops due to I_x that have no relation to the desired polarized potential. Referring to Figure 1,

the potential difference between J and M will be, in general

$$PD_J = PD_p \pm I_x R_s \qquad \text{(Equation 10)}$$

or, substituting for PD_p from Equation 6:

$$PD_J = PD_L \pm I_x R_f \pm I_x R_s = PD_L \pm I_x(R_f + R_s) \qquad \text{(Equation 11)}$$

According to Equation 10, PD_p may be calculated from PD_J if the term $I_x R_s$ can be evaluated. Similarly, Equation 11 shows that PD_L may be calculated from PD_J if the term $I_x(R_f + R_s)$ can be evaluated.

1.20 A number of techniques have been used by other workers to measure polarized potentials in the presence of impressed current. Some are designed to eliminate the undesired IR drops more or less automatically. Others are designed to evaluate the resistances so that the IR terms may be deducted algebraically. One method of the former type that has been devised for working with relatively large extraneous IR drops is known as the Pearson Bridge (Ref. 12). This bridge has been used with certain variations for a number of polarization studies relating to the action of corrosion inhibitors (Ref. 13 and 14). Holler (Ref. 9) modified the original circuit and used a somewhat different technique to study galvanic couples. Holler's technique was adopted for use in the present work because it was designed to eliminate the term $I_x(R_f + R_s)$ from the measured potential in a single operation and thus permit a relatively simple determination of PD_L. The details of this method are presented in Part 2.

1.21 Methods involving short-period interruption of polarizing current (Refs. 15, 16, 17, 18, 19) were considered, but were rejected for the following reasons. First, the electronic instrumentation required for best results using these methods is complex and might have been difficult to maintain in proper operating conditions.

Second, the widely distributed electrical system resulting from the continuous flow of brine (Ref. 20) would have severely limited frequency response of the network, and with it the rapidity with which the current could be switched on and off. And third, the interpretation of the data would have been difficult in view of the apparent lack of agreement between results obtained under even ideal conditions by workers in this field.

1.22 A third experimental approach involves measurement of the cell constants using alternating current techniques. Potentials are then corrected for resistive terms by calculation. This approach has the advantage that measurements may be made without making any abrupt changes in the D.C. polarizing current.

1.23 One of the earliest workers to use alternating current for this purpose was Reichenstein (Ref. 21), who determined the equivalent of R_f and C_f, Figure 1, and then subtracted the term IR_f from the potential difference measured in the presence of polarizing current to get the "true" potential. Many years later Wohr (Ref. 22) used superimposed A.C. to advantage, and recently Shaw and Remick (Ref. 23) and Haupin (Ref. 24) have made illuminating oscillographic studies using alternating current at a metal-solution interface. Results obtained substantiate the model of the interface as presented in Figure 1. The method appeared to be well suited to the type of work planned for this project, and eventually proved to be the only one which enabled the desired measurements to be made.

PART 2. APPARATUS AND PROCEDURES

2.0 The overall apparatus used to obtain the polarization data is shown as a block diagram in Figure 3. A description of the individual units is given below.

2.1 Solution Supply

2.1.1 Solutions were made up in 10 gallon glass bottles fitted with a solution outlet tube and a gas inlet tube terminating in a sintered glass dispersion disc. Carbon dioxide, commercial medical grade, was used without additional purification to purge solutions free of air.

2.1.2 Corrosive solution was pumped out of the storage bottles and through the remainder of the flow system by means of a finger-type pump which forced liquid through flexible tubing by a peristallic action.(1) Solution then flowed through glass coils immersed in a thermostated glycerine bath, by which it was brought to the desired temperature. Gas released from solution upon heating was vented to the atmosphere after the heating bath. Solution then flowed into the bottom of the test chamber, rose past the test electrode, and overflowed near the top of the chamber. When oil was used along with the water solution, it was prepared and delivered to the test chamber in the same manner.

2.2 Test Chambers

2.2.1 Two different types of test chambers were used during the work. The first to be used was a glass cylinder, 8 inches tall and 5 inches in diameter, having an internal volume of 2 liters (See Figure 4). The test electrode was located on the axis of the cylinder, while the auxiliary

(1) Sigmamotor Pump: Sigmamotor, Inc., Middleport, New York

electrode was in the form of a partial cylinder which completely surrounded the test electrode and was located just inside the wall of the chamber. A porous cylinder was placed between the inner and outer electrodes to prevent the mixing of gases from the cathode and anode processes, and to limit mixing of the electrolytes. The connection from the reference half-cell entered through a port half-way up the side of the chamber, passed through a hole in the auxiliary electrode, and terminated in the solution between this electrode and the porous cylinder.

2.2.2 Liquid and gas entered from a special premixing chamber attached to the bottom of the test chamber. This premixing device contained a rotary mechanical stirrer driven by a motor located beneath the unit, and was fitted with inlets for brine, oil, one or more gases, and one or more hypodermic needles used to inject chemical inhibitors into the flow stream immediately prior to contact with the electrode. This premixing chamber was attached to the glass corrosion cell by means of an O-ring seal, whereby it could be quickly detached for cleaning and inspection.

2.2.3 Electrical leads to the electrodes were brought out of the top of the corrosion chamber through gas-tight bushings sealed in a removable cover plate. This plate also carried the gas outlet tube from the central electrode space.

2.2.4 The second type of test chamber used was of the "H" shape, with one of the electrodes in each of the two vertical tubes (See Figure 5). Each vertical tube was 2 inches in diameter and 10 inches tall with an internal volume of 510 ml. The connecting tube was one inch in diameter, and contained a plug of glass wool.

2.2.5 The same premixing chamber as described above was used to introduce fluids into the right-hand arm containing the test electrode. The other arm was filled by flow of solution through the connecting tube. Other connections were similar to those of the above-described concentric arrangement, except that the probe from the reference half-cell entered through the top instead of the side. This H-cell is also shown in a photograph, Figure 6.

2.3 Test Electrode Assemblies

2.3.1 The size and shape of the test electrode was varied to suit the requirements of different experiments. During cathodic polarization runs, when the Corrosometer (see below) was used to measure metal loss, the electrode was made from shim stock 0.004 or 0.008 inches thick, was 1/8 inches wide by 3 inches long, and had an apparent exposed area of 5.8 sq.cm. This exposed specimen was an integral part of a transducer (called a "probe") made for use with the Corrosometer. Electrical connection to the polarization circuit was made by tapping one of the five electrical leads connecting the probe to the main unit of the Corrosometer. See Figure 6A.

2.3.2 During anodic polarization runs, when only hydrogen evolution was measured, the test electrode was made from a six inch length of 1-1/8 inch O.D. cold drawn steel tubing, SAE 1030, closed at both ends with a steel plug, and having a 1/4 inch O.D. steel tube attached axially to one end. The exposed area was adjustable up to approximately 80 sq.cm., by painting over a portion of the total available surface. The larger surface area was necessary to obtain sufficient hydrogen gas for accurate analysis within a reasonable length of time.

2.3.3 For special test runs in which metal loss and hydrogen evolution were measured simultaneously, an electrode was constructed by cementing a 2.5 cm. x 30 cm. strip of 0.002 inch shim stock to a 6 inch length of 1-1/4 inch O.D. Micarta tubing, in the shape of a spiral. Electrical leads were run through small holes in the wall of the tubing and thence out of the assembly through the hollow support tube.

2.4 Preparation of the Electrode Surface

2.4.1 Test electrode surfaces were prepared for all runs by sandblasting. This process served both to remove deposits left by previous use of the electrode, and to provide an active and uniformly etched surface for experimentation. No other kind of surface treatment, including acid etching, abrading with sandpaper or emerypaper, and pre-electrolysis gave results comparable to sandblasting with respect to reproduceability of potentials and time required for the potential and corrosion rate to become constant after immersion.

2.4.2 The sand used was 200 - 250 mesh, and was especially processed for use on small objects where maximum effect is desired with a minimum of metal removed. Measurement with the Corrosometer before and after blasting, indicated that good cleaning could usually be obtained with removal of less than 100 microinches of metal from the surface. The effect of wiping the sandblasted surface with tissue wet with organic solvents, in order to remove a small amount of grease deposited by the sand, was investigated. The result was usually a more erratic behavior than with no wiping at all. This effect was believed to be due to the presence of organic plastic coatings used on the electrodes to mask certain areas and protect electrical

connections. The solvents used probably dissolved small amounts of the coatings and spread the polymeric material over the metal surface, where it was removed only slowly by the action of the corrosive medium.

2.5 Exposure Conditions

2.5.1 The exposure conditions used for most of the runs reported here were as follows:

Flow Rate:	100 ml. per minute
Temperature:	60° C. (140° F.)
Solution:	3% NaCl in Distilled Water. Acetic Acid-Sodium Acetate buffer added. Saturated with Carbon Dioxide.
pH	4.5 or 5.5, as noted.

2.5.2 The throughput rate of 100 ml. brine per minute used for all the tests was quite low compared to that found in most industrial systems where corrosion due to mildly acidic brine is a problem. Hence, concentration polarization was expected to play a larger part in the total polarization effect observed during these experiments than it does in most applications. The problems of supplying large volumes of fresh solution for long periods of time in the laboratory ruled out throughputs higher than that used. The velocity of fluid flow relative to the metal surface was higher than would be calculated from the rate of throughput, because of the circular motion imparted to the fluids in the chamber by the impellor. Observation of the motion of gas bubbles led to the estimate of 10 to 15 cm. per second for the tangential fluid velocity at the surface of the test electrodes. This velocity was not great, but resulted in much less polarization than would have occurred had the solution been stagnant.

2.5.3 The pH range used (4.5 to 5.5) was chosen arbitrarily to fall within the weak acid range and yet give a corrosion rate high enough to work with. An acetic acid-sodium acetate buffer was used to stabilize the pH against changes due to (1) loss of CO_2 in the heating coils through which the brine passed, and (2) consumption of hydrogen ion by the corrosion process. The corrosion rate in this pH range is relatively low at room temperature, and so the elevated temperature was used to increase the corrosion rate, and also to increase the rate of adsorption and desorptions reactions at the metal-solution interface.

2.5.4 Oxygen was scrupulously avoided so that reduction of hydrogen ion would be the only known cathodic reaction occurring during the corrosion process. Thus, the rate of hydrogen evolution could be used whenever desired to measure the rate of corrosion.

2.6 General Procedure Used for Potential Runs

2.6.1 Certain operations common to all polarization potential runs are described here. Other more specific operations are described under individual headings.

2.6.2 Before the electrode surface was prepared, the solution supply pump was started and the test chamber filled with solution at the operating temperature. Several chamber volumes of solution were put through while a stream of CO_2 was used to purge the chamber. The electrode to be used was then sandblasted and immediately immersed in the test solution. The electrical connections were completed, and the corrosion rate and potential were followed until the potential reading was essentially constant. A drift

of less than 4 mv per hour was considered "constant." After the potential had been constant for about 30 minutes, the source of polarizing current was connected through the bridge circuit to the cell, and increasing values of current were passed between the two electrodes.

2.6.3 Three different procedures were used to determine the mixed potential polarization potentials, deperding on the behavior of the system. In one, referred to herein as Polarization Procedure A, the impressed current was applied at the desired intensity and the potential was followed until constant before recording its value. Once the potential corresponding to a given impressed current had been measured, the current was shut off and the potential again allowed to become constant. The next higher value of impressed current was then applied and the process repeated. In the second procedure, referred to as Polarization Procedure B, each higher value of impressed current was applied directly after the preceeding one, and time was allowed at each current for the potential to become constant. Polarization Procedure C involved measurement of the potential as soon as possible after each new value of impressed current was established, and the polarizing current was shut off after each measurement as in Procedure A.

2.6.4 The procedure followed when an inhibited system was to be tested was as follows. The test electrode was set up as described above and allowed to come to a constant uninhibited corrosion rate and potential ($I_x = 0$). A solution of the inhibitor was then injected by means of the automatic syringe, and injection continued until the corrosion rate was again constant at some new value. At least one hour of exposure to the inhibitor after the inhibited rate had become constant was allowed. The potential measurements were then

carried out as above. All data for inhibitors apply to measurements made during continuous injection of the inhibitor.

2.7 Apparatus for Measurement of Metal Loss

2.7.1 The apparatus used to measure loss of metal was a Recording Corrosometer.(1) This instrument follows the change of electrical resistance of a metallic specimen, and produces a chart record directly in units of microinches of metal lost from the surface. The basic principles of this general method have been described fully in the literature (Ref. 11, 25, 26).

2.7.2 The scale of the recorder was calibrated directly in terms of corrosion current in the following manner. A probe designed for use with the Corrosometer was first exposed to a neutral solution of sodium chloride in distilled water which had been freed of oxygen. The corrosion rate was followed for one hour, during which time no measurable corrosion occurred. A second electrode was then placed in the solution, and current was passed in such a direction that iron was dissolved from the test element surface. At all current densities up to 2 ma/sq. cm. (the highest tested), the metal loss indicated by the Corrosometer was within 5% of that calculated from the current using Faraday's equivalent. This accuracy was considered entirely adequate.

2.7.3 The conversion of anodic dissolution rate to electric current and vice versa was done using the following relationship (for mild steel):

$$\text{Current } (ma/cm^2) = (\text{microinches penetration/hr.}) \times 1.88 \times 10^{-2}$$

(1) Manufactured by Crest Instrument Company, Santa Fe Springs, California

2.8 Apparatus for Measurement of Hydrogen Evolution

2.8.1 The overall apparatus for continuous measurement of hydrogen gas from a corroding electrode has been described in the literature (Ref. 10). The essential components of the apparatus are (a) a source of sweeping gas, (b) a network of valves for directing the gases, (c) a Thermal Conductivity (T.C.) measuring device, and (d) a recording millivoltmeter to give a permanent record of the output of the measuring device.

2.8.2 The components used for the work were the same as those described in Ref. 10, with the exception of the recording millivoltmeter. A Brown "Electronik" Model 163, range 0 - 10 mv. D.C. was used for the work reported here. When the output from the T.C. device exceeded 10 mv., a 10,000 ohm[1] voltage divider was placed between the T.C. cell and the recorder. Operation of the recorder was satisfactory when so connected, even though working from an output impedance considerably higher than recommended, as the rate of change of input voltage was low.

2.8.3 The conversion of hydrogen evolution rate to electric current was done using the following relationship:

$$1.00 \times 10^{-2} \text{ cc. } H_2 \text{(at STP)/minute/cm}^2 \text{ surface} = 1.43 \text{ ma/cm}^2$$

2.9 Electrical Polarization Circuitry

2.9.1 Two different circuit arrangements were used for making potential measurements during the contract period. One was a combination of circuits

(1) This was the minimum resistance required to give less than 1% loading error when connected across the output of the T.C. cell used.

described by Pearson (Ref. 12) and Holler (Ref. 9), and was used for preliminary work with direct current only. The second circuit was a D.C. - A.C. impedance bridge, and was used for the greater part of the work.

2.9.2 The Pearson-Holler Bridge

2.9.2.1 The first of these two circuits is shown in Figure 7, and is essentially the same as that shown in Figure 3 of the proposal. R_1 was a precision resistor variable from 0 to 10 ohms in 0.1 ohm steps; R_2 was 220K ohms, 1%; R_3 was variable from 100K to 500K ohms, in 1,000 ohm steps. This arrangement of R_1, R_2, R_3 was chosen to facilitate computation of the value of the cell resistance in the fourth arm of the bridge, and to permit close balance of the bridge without having to make precise adjustments of R_1. In Holler's original circuit, all bridge balancing is done using R_1. In the present work, it was found that the cell resistance was so low that accurate adjustment of R_1 increments of the order of 0.01 ohm was necessary; thus making contact resistances and lead resistances critical. Instead of this, R_1 was set to the nearest ohm, and R_3 was used for a fine adjustment.

2.9.2.2 Sliders P_1 and P_2 together with B_1 provided a variable voltage source, with P_1 a coarse and P_2 a fine adjustment. The resistances of P_1 and P_2 were 100 to 200 ohms; and thus, the total effective resistance of arm CD was not measurably affected by the position of the variable taps of P_1 and P_2. The polarity shown at P_3 opposed that between the test electrode and the Calomel reference cell in the bridge. Potentiometer P_3 was a precision measuring device used to determine accurately the voltage between the adjustable taps of P_1 and P_2.

2.9.2.3 The detector was initially a Brown "Electronik" null detector in series with 100K ohm resistor. The resistor was necessary to avoid excessive loading of the bridge. This combination gave a maximum sensitivity of 0.1 mv. per millimeter scale deflection, with a zero stability of ± 0.05 mv. The overall response time was about 1/2 second. This device was satisfactory for measurement of slowly changing or constant potentials, but could not be used with transient voltages. For observation of transient behavior, an oscilloscope was used (Hewlett-Packard Model 130A).

2.9.2.4 The corrosion cell itself is shown schematically in Figure 7 connected to terminals B and E, with the test electrode connected to B. The Calomel electrode has its solution junction terminating in the electrolyte surrounding the electrodes, and the other terminal is connected to the bridge at C. Thus, the Calomel electrode and its internal resistance (R_4) form a part of the lower left arm of the bridge, in series with R_3. The Calomel electrode must pass a small current with negligible change of potential in this circuit, and so the unit was especially constructed to have a large mercury reservoir. The value of R_4 in the unit used was measured using an AC impedance bridge, and found to be 2400 ohms, including the capillary tube. This resistance was added to that of R_3, P_1, and P_2 to give the total resistance between D and F.

2.9.2.5 The circuitry outside the bridge between terminals A and E was used to supply a controlled polarizing current to the bridge. B_1 was a 90 volt pack of dry cell batteries capable of delivering up to 300 ma. for short intervals with no more than 10 volts interval drop. B_2 is a battery with a voltage adjustable to any selected fraction of B_1. Resistors R_6

and R_7 were used to prevent shorting of B_2 when switch S_2 is operated. R_8 is a variable resistor used to set I_x to any desired value. Switch S_1 disconnects the bridge for measurements at $I_x = 0$. Operation of Switch S_2 changes I_x by some selected amount at any point. Switch S_3 is used to open the bridge circuit. When S_3 was open, the combination of B_1, P_1, and P_3 with the Null Detector, comprised a potentiometric voltmeter that was used to measure PD_J.

2.9.2.6 The operation of this circuit during a run was as follows. With switches S_1 and S_3 open, the electrode was exposed until the reading on potentiometer P_3 (Detector at Null) was constant. The zero-impressed-current potential was then read on P_3. Switch S_1, was then closed and resistor R_8 was adjusted to pass the desired polarizing current through the bridge. The potential at P_3 corresponding to a Null at the Detector was followed until constant, then recorded as the uncompensated value of PD_J. Switch S_3 was closed and P_1 and P_2 adjusted to bring the detector close to mid-scale on the most sensitive scale. The position of S_2 was changed, and the deflection of the Detector immediately following the change of I_x noted. S_2 was returned to its original position, and after the bridge output was again constant, the switching of S_2 was repeated a number of times between which R_3 (and occasionally R_1) was adjusted for a minimum initial deflection of the Detector. When the best positions of R_1 and R_3 had been found, P_1 and P_2 were shifted to give a Null. The value of PD_L was then read on P_3. Thus, two potential readings were made at each setting of I_x.

2.9.3 The D.C. - A.C. Impedance Bridge

2.9.3.1 The second of the two types of bridge circuitry used was a combination D.C. and A.C. impedance bridge shown schematically in Figure 8. Resistors R_1 and R_2, and capacitor C_1 are components of the circuit assumed equivalent to that through which the polarizing current must pass in the test cell between the tip of the reference electrode junction and the metal of the test electrode, i.e., between J and M, Figure 1. The polarization cell is shown within the dotted lines with the test electrode connected to G, the system ground. The corroding interface plus part of the electrolyte resistance comprise the arm adjacent to the equivalent circuit, while R_4 plus part of the electrolyte resistance comprise the arm opposite the equivalent circuit. Resistance R_3 completes the bridge.

2.9.3.2 The values of these components depended on the area of the test electrode. Two sets of typical values are given in Table I below:

TABLE I

Typical Values for D.C. - A.C. Bridge

Component	Value For Apparent Area of 5 to 10 cm^2	Value For Apparent Area of 25 to 50 cm^2
R_1	300 - 3000 ohms	100 - 1000 ohms
R_2	10 - 100 ohms	5 - 50 ohms
R_3	20K - 100K	20K - 100K
R_4	500 ohms	100 ohms
C_1	4 - 40 mfd	40 mfd

2.9.3.3 The source of D.C. polarizing current consisted of a germanium diode rectifier and a two-section L-C filter, operating from the isolated secondary winding of a constant voltage transformer. This supply operated from 115 volts A.C. 60 cycles, and was capable of delivering up to 250 ma. D.C. at 100 volts or above. The current delivered to the bridge circuit was controlled with variable resistor, R_8. The sum of resistances R_8 and R_4 was kept at least 100 times the internal resistance of the polarization cell in order to provide constant polarizing current independent of variations in cell resistance.

2.9.3.4 Alternating current of variable frequency was supplied to the bridge by means of an audio signal generator. The output of the generator was connected directly to the bridge through blocking capacitor C_3. The amplitude of the A.C. signal was adjusted by means of the gain control on the generator chassis. This arrangement permitted up to 10 volts rms. A.C. signal to be applied to the bridge between point P and ground (G).

2.9.3.5 An oscilloscope was connected so that its horizontal axis input was connected to the junction of R_2 and R_3. Resistors R_6 and R_7 were found useful to suppress a certain amount of high frequency noise which otherwise decreased the accuracy of bridge adjustments. The input impedance of the scope was 1 megohm on each axis, so R_6 and R_7 introduced only about 10% loss of signal amplitude.

2.9.3.6 Figure 9 shows the arrangement of D.C. potential recording and indicating instruments used with the impedance bridge. P_2 was a recording millivoltmeter-potentiometer [1] with full scale equal to 10 mv. A special

(1) Brown "Electronik", Minneapolis-Honeywell Regulator Co.

input circuit was supplied by the manufacturer to present an input impedance of about 50,000 ohms, allowing the instrument to be used in relatively high resistance circuits without loss of sensitivity. This recorder was used in series with the adjustable bucking voltage generated by B_1, R_1, R_2, and P_1 to record variations in the test electrode potential. Potentiometer P_3 was a manually operated precision potentiometric voltmeter used to make accurate measurements after the potential had become constant.

2.9.3.7 Operation of the above circuit during a polarization run was as follows. With switch S_1 open and audio signal input at zero, the electrode is exposed under test conditions until the potential PD_J was constant, as indicated by the recording potentiometer P_2, Figure 10. Switch SW_1, Figure 10, was shifted to Manual, and PD_I was measured using P_3. To determine resistance and capacitance, the probe voltage from the Corrosometer was shut off, and a 50 cycle A.C. signal was impressed on the bridge to give 20 mv. peak to peak at the oscilloscope. The scope controls were set so that both horizontal and vertical inputs were displayed, and at the same gain. In general, the pattern was an ellipse with its major axis tilted to the horizontal. R_1, R_2, and R_3 were then varied to reduce the pattern to a single straight line and to set the angle of tilt at 45°. During these adjustments it was found convenient to hold C_1 constant. The frequency of the A.C. signal was then changed to 20 cps., the adjustment of R_1, R_2 and R_3 repeated to return the pattern to a 45° line, and the values of the variable resistors recorded. The above procedure was repeated at each value of I_x chosen for the run. Between each point where A.C. impedance

measurements were made, the audio frequency signal was turned off and the potential and corrosion rate were measured as described above.

2.9.3.8 The following relationships were used to calculate the values of R_f, and R_s from the data obtained by means of the bridges

$$R_f = \frac{R_1 \cdot R_4}{R_3} \qquad \text{(Equation 12)}$$

$$C_f = \frac{C_1 \cdot R_3}{R_4} \qquad \text{(Equation 13)}$$

$$R_s = \frac{R_2 \cdot R_4}{R_3} \qquad \text{(Equation 14)}$$

The values of PD_P and PD_L were then calculated from Equation 10 and 11:

$$PD_P = PD_J \pm I_x R_s \qquad \text{(Equation 10')}$$

$$PD_L = PD_J \pm I_x (R_f + R_s) \qquad \text{(Equation 11')}$$

PART 3. RESULTS

3.1 General Remarks

3.1.1 During the early stages of this study, both the test conditions and the electrical circuitry used to make potential measurements were modified a number of times in order to cope with the observed behavior of the corroding surface. Certain changes in procedure resulted in data that was somewhat different from that obtained previously. For this reason, the data obtained during the evolution of the final test procedures is considered questionable and is not presented here. Nevertheless, a number of observations made during the early work are of general interest and are so described below.

3.1.2 Initial experiments were carried out using solutions made with industrial tap water. The rate of throughput was lower than that used for later work, being only 25 cc. per minute. When cathodic current was applied to the electrode corroding under these conditions, several hours were required to obtain a stable potential reading. The potential drifted slowly in the anodic direction during this time and the rate of drift increased with increasing impressed current. When the electrode was removed from the solution after a run, a light colored powdery solid was found adhering to the surface. This proved to be mainly calcium carbonate with some magnesium and iron salts. Increasing the flow-rate from 25 ml. per minute to 50 to 100 ml. per minute did not appreciably change the amount of carbonate deposited or its effect on the potential. Lowering the pH of the solution from 5.5 to 4.5 decreased the amount of carbonate somewhat, but the potential behavior remained about the same. For this reason, distilled water was

substituted for tap water in the solution. No further trouble from this source was observed.

3.1.3 The effect of the pH and the flow rate of the solution on the time required for the potential to become constant - after applying polarizing current - was investigated. It was found that the lower the pH and the higher the flow rate, the more quickly the potential reached each new constant value. Much of the exploratory work was carried out at pH 5.5 and at a flow of 25 ml. per minute. These conditions were changed to pH 4.5 and flow of 100 ml. per minute for all the work done with the D.C. - A. C. impedance bridge.

3.1.4 Initial experiments were carried out using the concentric electrode arrangement (See Figure 4). Three different materials were tried as the auxiliary electrode. A Type 304 alloy steel screen appeared to work satisfactorily, but was discontinued when it was found that the electrical resistance of the test specimen decreased rather than remaining constant when sufficient cathodic current was passed to stop all loss of metal. This behavior was interpreted as indicating that metallic ions, dissolved off the alloy screen by the anodic current there, were diffusing through the porous divider and were being reduced on the test electrode surface.

3.5.5 A piece of mild steel shim stock was substituted as the outer electrode. No obvious difficulties were experienced with this material. However, the concentration of dissolved iron in both compartments of the cell was much higher than desirable when both electrodes were mild steel. It was felt that the high iron concentration might lead to non-representative polarization behavior, but no reliable data was obtained to substantiate this due to the difficulties with the bridge circuit described below.

3.1.6 The third material tried for the auxiliary electrode was platinum foil. Here the only undesirable by-product of electrode activity was oxygen generated when the platinum was made the anode in the polarization cell. To minimize the possibility that dissolved oxygen from the anode chamber would reach the central electrode, the test solution was flowed rapidly through the annular space between the porous cylinder and the outer electrode. In spite of the precautions taken, the potential behavior and appearance of the test electrode indicated that oxygen was being reduced during cathodic polarization.

3.1.7 From these results, it was concluded that the concentric electrode arrangement as originally set up could not be used for polarization studies because of unavoidable mixing of anode and cathode products through the porous membrane. Hence, despite its advantages of symmetry and current distribution, the concentric type cell was replaced by the H-shaped cell described in Section 2.2.4. Those potential measurements that were made with the concentric arrangement were made using the modified Pearson-Holler bridge circuit. The results of this work are described in the following section.

3.2 Results From Work with the Pearson-Holler Bridge

3.2.1 A number of cathodic runs were made on uninhibited steel electrodes using the Pearson-Holler Bridge. The general operation of the circuit was as expected, but the accuracy of the resistance setting was poor. The inaccuracy resulted from two characteristics of the cell being studied:

(1) The effective interface resistance R_f was low, resulting in a proportionately low $I_x R_f$ term; and (2) The output of the bridge (at constant I_x) fluctuated, due apparently to fluctuations in the potential difference across the metal-solution interface.

3.2.2 When I_x is changed by ΔI_x as is done to obtain a resistive balance, the error signal output due to resistance unbalance only is given by[1]

$$\Delta V_R = \frac{\Delta I_x \cdot \Delta R}{2} \qquad \text{(Equation 15)}$$

where $\Delta R = R_2(R_5 + R_f) - R_1(R_3 + R_4)$, Figure 7. The range of I_x in the region of local cell corrosion was from 0 to 20 ma., and the resistance corresponding to $R_5 + R_f$ was approximately 1 ohm. Thus, even through the resistance setting might have been in error by as much as 100% (ΔR = 1 ohm), the error signal that would have been produced by a 10% change in I_x would have been a maximum of 2 mv. To have achieved 10% accuracy in resistance setting would have required detection of 0.2 mv. Reliable detection of such signals would have been a matter only of appropriate instrumentation had it not been for the fluctuations in bridge output mentioned above. The latter occurred in a random manner with a maximum amplitude which was proportional to I_x. For this reason, they were believed due to fluctuations in the effective interface resistance.

3.2.3 From previous exploratory work it was known that the reduced mixed potential (PD_L) of steel under the test conditions changed only slightly from its zero-impressed-current value until the net local anodic current approached zero. Thus, it was reasoned, within this region I_x might be

(1) The expressions for error signals for this bridge are different from those for a conventional Wheatstone Bridge, because here $R_1 + R_5 \gg R_5 + R_3$, and the bridge operates under constant current rather than constant voltage.

changed by a relatively large amount without causing a significant shift in the potential component of the total potential difference, PD_J. Accordingly, the circuit was altered so that operation of S_2 produced a change of 10 ma. in I_x regardless of the base value of I_x. This procedure resulted in an error signal due to resistive unbalance that was large enough to detect above the background. However, another type of interference was introduced by the larger current increments: Immediately following the initial, instantaneous change in output due to resistance unbalance, an only slightly less rapid change in output occurred which continued for several seconds at a rate which decreased with time. This behavior occurred in reverse when the original current was resumed. One possible explanation for this behavior is presented in the Discussion.

3.2.4 When I_x was increased beyond the point where local anodic action stopped, and thus, where the surface behaved like a hydrogen electrode, the step-change in I_x used to balance the bridge was held to a maximum of 10 ma. regardless of the value of I_x. As a result, the maximum probable error in the reduced potential determined using this method was ± 4 mv. in the region where the potential changed very little with a change of I_x, and ± 20 mv. where potential changed considerably with applied current. This order of accuracy was sufficient for rough survey work, but did not permit detection of small charges in the potential or in R_f.

3.2.5 In order to facilitate operation of the bridge and the D.C.-shift balancing technique in the presence of the above-mentioned transients, the sensitivity of the detector was greatly reduced and the resistance settings were made by adjusting the resistance at each point to a value

that was half way between settings that gave equal but opposite error signals large enough to be easily separated from interference signals. By this means, a number of cathodic runs were carried out with the Pearson-Holler bridge. In spite of these efforts, however, the data obtained was of questionable reliability, and so it is not reported.

3.2.6 The difficulties encountered in the use of the Pearson-Holler bridge as described in the foregoing sections led to the development of the D.C.-A.C. impedance bridge, by means of which the cell resistances could be measured without having to make sudden changes in the polarizing current. In addition, the H-shaped test chamber was substituted for the concentric chamber at about the same time the new bridge circuit was put in use. Section 2.3 describes these units and discusses the relative merits of the two chambers.

3.2.7 No anode - cathode mixing or other interferring phenomenon appeared to take place in the H-cell. Following immersion of an electrode with a freshly-sandblasted surface in the test solution, the potential moved in the anodic direction (increasingly negative) for 10 to 15 minutes, reached a maximum anodic value, then began to move in the cathodic direction for a period which varied from 30 minutes to 2 hours. The rate of drift was in the range of 10 to 15 mv. per hour. This behavior occurred every time and was generally reproduceable except for the time factor. If time was not allowed at the beginning for the zero-impressed-current potential to reach its most cathodic point, all subsequently measured potentials were found to drift for a considerable time in the cathodic direction. During cathodic runs, the direction of this drift was opposed to that of the shift from the main effect of current on the interface, and the net result was confusing and misleading.

3.2.8 Careful observation [illegible]rect potential (PD_p) in the presence of impressed current showed the following. After the impressed current increased from one value to another, there was always a period following the initial rapid change of potential, during which the potential changed relatively slowly before becoming constant. This period lasted only about 30 seconds or less in most experiments. During cathodic polarization, the drift was in the anodic direction when I_x was less than that required to stop local cell action, and in the opposite or cathodic direction when I_x was greater than this value. During anodic polarization, the direction of the drift was toward more anodic values throughout the range of I_x tested. This behavior is due to changes in the interface resistance.

3.3 Results Using the D.C. - A.C. Impedance Bridge

3.3.1 The operation of the impedance bridge for the measurement of interface resistance and capacitance is described in Section 2.9.3. The circuit is shown in Figure 8. With the oscilloscope used, the best combination of signal-to-noise ratio and precision of bridge balance was obtained by setting the gain of each input channel to the "2 mv. per cm." position and generating an input signal of 16 and 20 mv. peak to peak at each channel. This voltage is measured between the tip of the reference electrode capillary and the test electrode, and thus almost all of it appears across the interface resistance.

3.3.2 Tests were made to determine whether the impressed alternating voltage would have any undesirable affect on the interface. No change in any of the measureable properties of the interface was detected after exposure of an uninhibited surface to 20 mv. at 100 cps. and at 20 cps. for periods

up to 30 minutes. The impressed voltage was gradually increased at 20 cps until at around 100 mv. the direct mixed potential began to move in the anodic direction. When the A.C. voltage was reduced to below 50 mv., the potential rapidly resumed its original value. The corrosion rate was not measured during this test. From the results obtained it was concluded that 20 mv. A.C. across the interface would not noticeably alter the resistance, capacitance, or electrode potential.

3.3.3 A considerable number of cathodic polarization runs were made on uninhibited electrodes using the D.C. - A.C. bridge. Multiple runs were found necessary to develop the technique of operating the bridge, and to obtain sufficient data to indicate the reproduceability of results. Somewhat better results were obtained by Polarization Procedure A (Section 2.6.3), in which the impressed current was returned to zero between each measurement, than were obtained using Polarization Procedure B. However, Procedure A was much more time consuming, especially when the potential drifted after changes in I_x.

3.3.4 Table II presents the data from a typical cathodic run on an uninhibited surface using Polarization Procedure A. A plot of these data is shown in Figure 10. The horizontal axis of this diagram, and of all other mixed potential polarization diagrams presented here, is laid off in units of the logarithm of the apparent density of impressed current. The semi-log presentation is used to show the behavior of the potentials clearly over a wider range of impressed current than would be possible using a linear current scale.

TABLE II

DATA FROM A TYPICAL CATHODIC POLARIZATION RUN

Apparent Current Density $\bar{I}_x$ (ma/cm^2)	PD_p v. vs. SCE*	$\bar{C}_f$ mfd/cm^2	$\bar{R}_f$ ohm/cm^2	Corrosion Rate mdd**
0.0	-0.722	1320	9.2	2550
0.412	-0.726	1280	10.2	2120
0.825	-0.732	1220	12.2	1710
1.28	-0.740	1160	14.8	1220
1.65	-0.755	1080	20.3	840
2.06	-0.787	980	28.3	435
2.47	-0.882	940	30.1	0
3.00	-0.957	840	28.9	-
3.50	-0.995	860	24.5	-
4.12	-1.041	860	21.5	-
5.15	-1.073	860	16.8	-
6.40	-1.103	900	13.0	-
7.20	-1.119	920	11.0	-
8.25	-1.135	920	10.0	-

** milligrams per square decimeter per day

* The sign of all potentials in this report is governed by the convention which makes the standard metallic zinc electrode potential negative.

3.3.5 The term "apparent current density" is defined as the total current divided by the total apparent area receiving that current. Unless specifically stated otherwise, all current densities, either of impressed current or of local cell current, used in this report will be apparent densities as defined. These values are designated by placing a horizontal bar over the symbol for the desired current. In a like manner, any other quantity that relates to a unit of apparent area (one square centimeter) is shown with a bar over the usual symbol.

3.3.6 For purposes of comparison, a plot of results from a representative run made on an uninhibited surface using Polarization Procedure B (Section 2.6. is shown in Figure 11. The tabulation of actual measured values corresponding to these curves is omitted, inasmuch as the exact values are not significant in view of the variation observed from one run to another.

3.3.7 The shape of the curves in Figures 10 and 11 are seen to be quite similar. The following observations may be made about both.

(1) PD_L constant at its zero-impressed-current value until I_x approaches the point where $i_A = 0$.

(2) PD_L and PD_p change most rapidly at or very near the point where $i_A = 0$. A point of inflection in both curves occurs where $i_A = 0$.

(3) The curve for PD_L is not a straight line on the semi-log plot in the region where the surface is presumably entirely cathodic. The deviation from the straight line drawn tangent to the curve at the point of inflection is in the direction of too small a change of potential with increasing I_x.

(4) The interface resistance $\bar{R}_f$ passes through a maximum at or near where $i_A = 0$.

(5) The interface capacitance C_f decreases slowly at low I_x, then more rapidly to a broad minimum at values of I_x slightly greater than that required to reduce i_A to zero.

3.3.8 The portion of the curves of Figures 10A and 11A used to construct the local anodic polarization curves lies to the left of the dotted vertical line marked $i_A = 0$. The values for local anodic current in this region were calculated from the rate of metal loss measured at different points along the curve. To obtain data that would be of assistance in the estimation of local anode currents when for some reason the corrosion rate could not be measured directly during a potential run, several additional experiments were carried out in which only currents and corrosion rates were measured. It was hoped that some general relationship between i_A and I_x would be found. The data from the best two of these runs is shown in Table III. Note that the ratio of $(\bar{I}_x)_{i_A=0}$ to $(\bar{i}_A)_{I_x=0}$ is 1.75 in Run No. 1 and 1.48 in Run No. 2. This ratio is 2.5 from the data of Table II (Figure 10) and 1.9 from the data of Figure 11. The reason for this variation, and its significance, are not known at this time. Certain possible contributing factors are discussed in Part 4.

3.3.9 The data of Table III is presented in graphical form in Figure 12. Data for i_A is plotted as a fraction of its value at $I_x = 0$, whereas data for I_x is plotted as a fraction of its value at $i_A = 0$. In this way the figure is made useful with any values of $(\bar{i}_A)_{I_x=0}$ and $(I_x)_{i_A=0}$.

3.3.10 Local anode polarization curves derived from the data of Figures 10 and 11 are shown in Figures 13 and 14, respectively. Both PD_p and PD_L are plotted, the latter being shown as a dotted line. The scale for i_A in these diagrams was made linear instead of logarithmic for two reasons: (1) The linear scale is proportional to the (average) corrosion rate on the surface; and (2) The point at $i_A = 0$ can be shown on the linear scale but not on a log scale. These curves are discussed more fully in Part 4.

TABLE III

LOCAL ANODIC CURRENT DATA

	Impressed Current, I_x		Corrosion Rate	Local Anode Current, i_A	
	ma/cm^2	% of $(I_x)_{i_A=0}$	mdd	ma/cm^2	% of max.
Run No. 1	0	0	2360	0.90	100
	0.74	47	1230	0.47	52
	0.90	59	940	0.36	40
	1.10	71	720	0.27	30
	1.48	94	129	0.05	5.5
	1.57	100	0	0	0
Run No. 2	0	0	2770	1.06	100
	0.56	35	1740	0.67	63
	0.74	47	1460	0.56	53
	0.93	59	1130	0.43	41
	1.11	71	800	0.30	21
	1.35	86	360	0.14	13
	1.60	100	0	0	0

3.4 Anodic Polarization-Uninhibited Electrode

3.4.1 Anodic polarization of uninhibited specimens resulted in a potential behavior considerably different from that noted during cathodic runs. The potential usually required only a few minutes to become constant after each new value of I_x was applied. On the other hand, if and when I_x was shut off between measurements, the $I_x = 0$ potential was found to have shifted in the anodic direction, from which it recovered only slowly in the absence of impressed current.

3.4.2 Data from a typical anodic polarization run using continuous application of anodic polarizing current is shown in Table IV. The curves are shown in Figure 15. The following points may be made about these data:

(1) There was little if any region of I_x wherein PD_L was constant, although the rate of change was very small below $\bar{I}_x = 2$ ma/sq. cm.

(2) Both PD_L and PD_P change gradually over a broad range of $\bar{I}_x$ ($\bar{I}_x = 4$ to 40 ma/sq. cm.) below that which was necessary to reduce i_C to zero. This is in contrast to the relatively sharp break in PD_L near $i_A = 0$ on the cathodic polarization curve (e.g., Figure 10).

(3) No linear portion of the data is to be expected in Figure 15A, inasmuch as some local cathodic activity is present throughout the range of $\bar{I}_x$ shown.

(4) The magnitude of I_x required to reduce i_C significantly is much greater than that required to reduce i_A to zero during cathodic polarization.

(5) The interface resistance decreased throughout the range of $\bar{I}_x$ shown. The interface capacitance increased very slowly below $\bar{I}_x = 2$ ma/cm^2, then rapidly at higher current density.

TABLE IV

ANODIC POLARIZATION DATA - UNINHIBITED SURFACE

Apparent Current Density $\bar{I}_x$ (ma/cm^2)	PDp (mv.)	$\bar{C}_f$ (mfd/cm^2)	$\bar{R}_s$ (ohm/cm^2)	$\bar{R}_f$ (ohm/cm^2)
2.04	-686	840	1.8	7.0
4.15	-656	920	1.8	4.6
6.17	-632	1060	1.8	4.0
10.6	-599	1240	1.7	2.9
24.0	-544	-	-	-
40.8	-505	-	-	-

3.4.3 An emperical relationship found between $\bar{i}_C$ and $\bar{I}_x$ is shown in Figure 16. The values of $\bar{i}_C$ were calculated from hydrogen evolution data as described in Section 2.8.3. The values for $\bar{i}_C$ may be seen to form a straight line when plotted against log $\bar{I}_x$. A fractional scale is used for each axis to facilitate use of the chart with any values of $(\bar{i}_C)_{max}$ and $(I_x)_{i_C=0}$.

3.4.4 The value of $(I_x)_{i_C=0}$ was determined only indirectly. This was necessary because of the excessively large amount of current required to reach the point where $i_C = 0$. Current densitites up to 40 ma/sq. cm.

were applied, but resulted in less than 75% reduction of local cathodic current. To have been able to apply higher current densities would have required considerable modification of the apparatus. Instead, the data up to $\bar{I}_x$ = 40 ma/sq. cm. was plotted on semi-log paper, and the points appeared to fall close to a straight line. The value of I_x necessary to reduce i_C to zero, i.e., $(I_x)_{i_C=0}$, was taken as the i_C = 0 axis intercept assuming that the log relation continued to hold. This intercept occurred at approximately $\bar{I}_x$ = 150 ma/sq. cm. for the conditions under which Figure 15 applies.

3.4.5 The range of values found for $(i_C)_{max}$ (i.e., the value of i_C when I_x = 0) was from 0.9 to 1.2 ma/sq. cm. for several different runs. Thus, the ratio of $(I_x)_{i_C=0}$ to $(i_C)_{max}$ was in the range from 120 to 170 for this electrode system. This ratio is very much greater than the ratio of $(I_x)_{i_A=0}$ to $(i_A)_{I_x=0}$ found for cathodic polarization behavior. The significance of this large ratio is discussed in Part 4.

3.4.6 The estimated value of 150 ma/sq. cm. for $(I_x)_{i_C=0}$ lies well beyond the highest value $\bar{I}_x$ shown in Figure 15A. Thus, the potentials corresponding $\bar{I}_x$ from 40 to 150 ma/sq. cm. were not measured. Instead, the curve for PD_L was extended at constant curvature to the point where $\bar{I}_x$ = 100 ma/sq. cm. then with increasing curvature to $\bar{I}_x$ = 150 ma/sq. cm. The curvature was assumed to increase in this latter region near where i_C = 0 by analogy to the behavior of PD_A near i_A = 0 as shown in Figure 11A.

3.4.7 The resulting local cathodic polarization curve is shown in Figure 17. It may be seen that the experimentally measured potentials lie on a smooth curve when plotted on a linear i_C scale. The portion of the curve for PD_P derived from estimated data is shown dotted. The curve for PD_L is

quite similar to that for PD_p, and does not exhibit any characteristics not shown by that for PD_p. The region of maximum uncertainty lies within the first 10% of the range of i_C, and thus, does not seriously affect the shape and position of the curves as a whole. The uncertainty in this region does affect the $i_C = 0$ axis intercept, however. This intercept is seen to occur somewhere between -300 and -350 mv. vs. S.C.E. for PD_p.

3.5 Polarization Measurements on Inhibited Surfaces

3.5.1 The general procedure used for polarization runs in the presence of corrosion inhibitors is described in Section 2.6.4. Data reported applies to measurements made during continuous treatment with each inhibitor. Originally, it was planned to make the measurements on the films resulting from the action of inhibitors after the chemicals in solution had been flushed from the chamber. It was found, however, that as soon as continuous injection of certain of the inhibitors tested was stopped, the potential and the corrosion rate began to drift in the direction corresponding to the uninhibited state. With certain types of inhibitors the drift was small and the potential and corrosion rate soon became stable again; with other types the drifts continued indefinitely. Similar drifts were encountered when attempts were made to make measurements on surfaces only partially covered with an inhibitor film. A number of runs were carried out by adjusting the concentration of inhibitor during the injection period so that the corrosion rate levelled off at from 25 to 75% of its original value. It was found that under these conditions the potential (no applied current) continued to change in the cathodic direction, i.e., that corresponding to a greater degree of inhibition even though the measured corrosion

rate appeared to be constant. Prolonged observation showed that the corrosion rate was decreasing slowly. It was very difficult to produce a truly constant state at any degree of inhibition between zero and whatever maximum effectiveness was characteristic of the concentration of inhibitor tested.

3.5.2 Data for construction of mixed potential curves, i.e., I_x and PD_p were determined during inhibited runs using the same technique that was used during uninhibited runs. Unfortunately, however, the dependence of i_A (or i_C) on I_x, required to convert mixed potential data to local cell polarization data, could not be determined with any useable degree of accuracy during runs where effective inhibitors were used. This was because of the very low corrosion rates involved and the limited time that could be spent at each data point. Despite the great sensitivity of the recording Corrosometer used to measure corrosion rates (resolution: 0.1 microinch), the total uncertainty in this type of measurement was such that, at corrosion rates of less than 1.0 microinch, at least one hour under constant conditions was required before one could say with certainty that the rate was constant, and before a precise measurement of the rate could be determined from the chart record.

3.5.3 As described below, the application of impressed current to surfaces bearing inhibitor films produced certain irreversible effects which varied with time; these effects were especially severe during anodic polarization. Thus, it was felt that exposure to polarizing current for periods of one hour or longer would not necessarily produce a constant corrosion rate at the end of that time. Furthermore, the potential and corrosion rate after long

periods of time may not bear any direct relation to the condition of the surface as it existed before the waiting period. Therefore, every attempt was made to measure the potential as soon as possible after applying the external current, waiting only for any rapid changes in potential following changes in I_x to subside.

3.5.4 In order that the mixed potential data for each inhibitor might be transformed into the desired local cell polarization data, a relationship between i_A or i_C and I_x during polarization of the inhibited surface was estimated, as follows. For cathodic polarization, it was assumed that i_A varied linearly with I_x in the same manner as for the uninhibited surface as shown in Figure 12. For anodic polarization, it was assumed that i_C varied linearly with log I_x as shown in Figure 16. In either case, the value of $(i_A)_{max}$ or $(i_C)_{max}$ used was that calculated from the inhibited corrosion rate when $I_x = 0$. Values for $(I_x)_{i_A=0}$ were difficult to measure directly with any accuracy during the runs because of the contingent difficulty in determining the exact point when i_A or i_C was equal to zero. When no other data was available, $(I_x)_{i_A=0}$ for the inhibited state was approximated by assuming that it was equal to twice $(i_A)_{max}$, as found for the uninhibited surface. In a like manner $(I_x)_{i_A=0}$ was approximated by assuming that it was equal to 100 $(i_C)_{max}$. Once these values had been calculated, Figures 12 and 16 were used to determine intermediate points as desired.

3.5.5 Two different ways of presenting local cell polarization diagrams for inhibitors are used. One is a plot of polarized local half-cell potentials vs. local cell current. This type is shown in Figure 21. Here the curves for all four of the inhibitors for which complete curves were available are superimposed in order to permit a direct comparison to be made between the slopes and positions of anode and cathode lines. The other type of local cell diagram, shown in Figures 22 through 25, presents the potential data for each inhibitor separately as a function of the applicable percentage of the maximum local cell current (that which flowed in the absence of applied current) observed for that inhibitor. Thus, in this latter type of diagram, the intersection of the anodic and cathodic curves is always the same distance (100 percentage units) from the vertical axis, regardless of the actual value of the current at this point.

3.5.6 Runs involving corrosion inhibitors were characterized by potentials that were often markedly non-reproduceable, in spite of all attempts to repeat experiments under identical conditions. For this reason, at least three runs were made under any given set of conditions, and the best set of data was selected as being representative. The potential behavior was often so different from one run to the next that no statistical grouping or averaging could be applied to improve the data.

3.5.7 The inhibitors tested in this study included only those that were either completely soluble or easily dispersible in 3% sodium chloride solution at concentrations up to several hundred ppm. The soluble members included sodium chromate, sodium ferrocyanide, sodium arsenite, and acetic acid salts of certain long-chain amines in alcohol solution. The dispersible members consisted of solutions of long-chain amine salts in hydrocarbon solvents, and a thiourea-formaldehyde condensation product. No attempt was made to

compare the various inhibitors on any equal weight or concentration basis. Rather, the concentration used was usually adjusted as found necessary to produce a minimum of 85% inhibition in a reasonably short time. Thus, whatever comparison might be made would be at about the same degree of inhibition for each.

3.5.8 Results with Sodium Chromate

3.5.8.1 Sodium chromate has a reputation of being an "anodic" inhibitor when used in neutral or alkaline media in the presence of oxygen. An "anodic" inhibitor is one which produces its effect by causing the local anodes to be polarized more strongly than local cathodes, thus bringing the corrosion process under anodic control. There is available almost no information on the use of chromate as an inhibitor in acid solutions. It is clear that in strong acids chromate is an accelerator and not an inhibitor (Ref. 27). In weak acids (pH 4 to 6) inhibition may be observed under certain conditions. Tests were therefore made using sodium chromate in an attempt to shed more light on the mechanism of inhibition in acid solution.

3.5.8.2 Initial testing was begun at 50 ppm sodium chromate in a solution buffered at pH 5.5. The initial effect was a three-fold increase in the corrosion rate, accompanied by a shift of potential in the cathodic direction. After injection at 50 ppm had been continued for one hour, during which time little change in the accelerated rate was observed, the concentration was increased to 100 ppm. There was no immediate change in the corrosion rate, but after about 30 minutes the rate began to decrease slowly. After about

four hours the rate had decreased to 15% of its original value, and had begun to level off. At this point, the interface resistance, interface capacitance, and mixed potential were measured. Representative data from one such run are given in Table V.

3.5.8.3 When a cathodic polarizing current of 10^{-2} ma/sq. cm. was applied to the inhibited surface, the potential underwent a rapid shift in the anodic direction, then drifted slowly toward more negative (more anodic) values over a long period of time. When the polarizing current was shut off, the potential changed only very slowly toward its original value. This behavior indicated that the impressed current was causing essentially irreversible changes at the surface that were not related to the properties of the surface at the time the current was applied. Repeated attempts to obtain stable potential readings in the presence of polarizing current were not successful. For this reason it was decided to discontinue the investigation of sodium chromate in order to devote more time to inhibitors that might give more straightforward results.

3.5.9 Results with Sodium Ferrocyanide

3.5.9.1 Sodium ferrocyanide was tested as an example of an inhibitor which presumably functions by forming an insoluble compound by reaction with iron or ferrous ion at the metal-solution interface. Concentrations up to 50 ppm, calculated as the anhydrous salt, $Na_4Fe(CN)_6$, caused only a small decrease in the corrosion rate in a 4 hour period under the test conditions. A concentration of 200 ppm was necessary to reduce the corrosion rate rapidly, and resulted in 90-95% inhibition within 4 hours. The surface of the electrode was blue at this point. Interface resistance, capacitance, and potential data for one typical run are given in Table V.

TABLE V

SUMMARY OF TYPICAL DATA FOR DIFFERENT INHIBITORS

	INHIBITOR	ACTIVE CONCENTRATION ppm	UNINHIBITED CORROSION RATE mdd	INHIBITION %	INTERFACE RESISTANCE (ohm/sq.cm.) Before	INTERFACE RESISTANCE (ohm/sq.cm.) After	INTERFACE CAPACITANCE (mfd/sq.cm.) Before	INTERFACE CAPACITANCE (mfd/sq.cm.) After	MIXED POTENTIAL (v. vs. SCE) Before	MIXED POTENTIAL (v. vs. SCE) After
1	Sodium Chromate	100	3380	85	6.90	25.0	1,856	400	-0.722	-0.665
2	Sodium Ferrocyanide	100	1500	95	23.40	145.0	1,488	1,024	-0.715	-0.675
3	Sodium Arsenite	50	2420	98	6.25	165.0	2,880	608	-0.722	-0.652
4	Subst. Imidazoline	100	2920	93	11.75	131.5	1,088	608	-0.725	-0.613
5	Subst. Imidazoline plus oil	100	1750	98	18.0	166.0	688	180	-0.722	-0.615
6	Thiourea - HCHO Condensation Product	50	2680	95	12.7	130.0	912	336	-0.724	-0.632

3.5.9.2 Cathodic polarization was begun by using a test current of 0.05 ma/sq. cm. to check the general reaction of the interface. Immediately following the application of current, a shift of potential to a more anodic value and a decrease in corrosion rate took place as expected. Following these initial changes, the potential continued to move toward more anodic (increasingly negative) values and the corrosion rate continued to decrease as long as the polarizing current was flowing. These drifts were followed for about one hour, during which there was no indication that conditions would become stable. At the end of this time, the impressed current was shut off, whereupon the corrosion rate remained fairly constant at the same value as in the presence of impressed current, which was about 25 to 30% lower than the rate before current was applied. It was evident that the polarizing current had caused relatively large changes in the interface, thus making the desired polarization measurements difficult to make.

3.5.9.3 The results of several additional cathodic runs with sodium ferrocyanide were essentially the same as those described above. Because of this unstable behavior, an attempt was made to measure the potential at only one point on the curve: that where I_x is just sufficient to reduce i_A to zero. The required value of I_x was estimated as being twice the inhibited local cell corrosion current. This amount of current was applied and the new potential was measured as soon as possible thereafter. During the time required for the measuring circuit to be adjusted to measure the polarized potential, which was about 10 seconds, a shift of 57 mv. had taken place. The potential was continuing to change at a rate of 2 to 3 mv. per minute at this point. The applied current was maintained for 20 minutes, which was long enough to permit a reliable measurement of the corrosion rate.

This proved to be essentially zero. During the 20 minute period the potential changed by an additional 17 mv., so that the total was 74 mv. It appears that the difference in potential between the point where $I_x = 0$ and that where $i_A = 0$ probably lies somewhere between 60 and 85 mv. Because of the lack of data, no mixed potential cathodic polarization curve is shown for this inhibitor.

3.5.9.4 A limited effort was made to obtain anodic polarization data for sodium ferrocyanide. A concentration of 200 ppm was injected to reduce the corrosion rate rapidly. After three hours the rate was 15% of the original. The injected concentration was reduced to 100 ppm and anodic current was impressed at 0.1 ma/sq. cm. After an immediate shift of the potential in the cathodic direction, there was a relatively rapid drift in the anodic direction. This was accompanied by a rapid decrease in the interface resistance and an increase in the local cell corrosion rate. When I_x was shut off, the potential remained more anodic than before I_x had been applied, and the local cell corrosion rate remained higher than before. Each of these then slowly changed toward their original values as the inhibitor was again adsorbed on areas from which it had been removed. An idea of the speed with which the interface was altered by anodic impressed current was obtained by repeating the above experiment with the interface resistance and capacitance instruments in continuous operation. With no impressed current flowing, the bridge circuit (Section 2.9.3) was adjusted to give a single straight line on the oscilloscope. The polarizing current was then switched on while observing the scope display. Immediately upon application of impressed current the line on the CRT face began to open up into an ellipse. Rapid readjustment of the bridge components to measure the new interface values indicated that a 10 to 15% decrease of R_f, and a

corresponding increase in C_z, had occurred during the first 5 to 10 seconds after the polarizing current was applied. When this current was shut off, there was no immediate change on the CRT screen, showing that a change in the interface had been produced which persisted after current no longer flowed.

3.5.9.5 Because of this type of instability no attempt was made to determine a complete anodic polarization curve for sodium ferrocyanide. Instead, the potential was measured at only two points: (1) at I_x = 10 times the equilibrium inhibited local cell current, $(i_C)_{I_x=0}$; and (2) at I_x = 100 $(i_C)_{I_x=0}$, at which i_C should have been at or near zero. Polarization Procedure C was employed to expose the interface for the smallest possible time to the impressed current. Measurements were repeated several times and the results averaged. The figures, expressed as the difference between the zero-impressed-current value and the polarized value, and as a range within which the "true" value probably lies, were: (1) 30 - 50 mv., and (2) 70 - 100 mv., respectively.

3.5.9.6 Local cell polarization diagrams for sodium ferrocyanide, drawn from the available data, are shown in Figures 21 and 22. Only the end-points of the curves, i.e., the initial mixed potential and open-circuit (zero local cell current) potentials, were known to any degree of certainty, so the construction merely involved drawing lines between these points. In Figure 21 the curves are shown as single dotted lines (labelled A-1 and C-1) for the sake of simplicity. In Figure 22 anodic and cathodic "curves" are shown as regions bounded by dotted lines. These regions are drawn in such

a manner that the probability that the "true" curve lies outside them is quite low. The local cathode polarization region takes into account a possible error of ± 50% in the estimated local cell current, which as described above, could not be measured directly because of the instability of the inhibitor film. In spite of the resulting dispersion of the data, it may be seen that the trend is well defined and allows definite conclusions to be drawn from the figure. These are discussed in Part 4.

3.5.10 Results with Sodium Arsenite

3.5.10.1 Sodium arsenite has been used for many years as an inhibitor for both strong and weak acid corrosion. The general mechanism is believed to involve reduction to elemental arsenic and consequent "poisoning" of the hydrogen electrode half-reaction on the steel surface. This action would make arsenite primarily a "cathodic" inhibitor, and should be revealed by the shape of the local cell polarization diagram.

3.5.10.2 Sodium arsenite was studied in solutions at pH 4.5. Injection of 50 ppm calculated as $NaAsO_2$ produced a rapid change in the potential toward more cathodic values. The decrease in the corrosion rate followed the change of potential with a lag of 15 to 20 minutes. This lag was not due to instrument response, as there is no lag in the response of the Corrosometer (although a period of about 15 minutes is usually required to establish positively that a change in corrosion rate had occurred at the beginning of this time period). In the above experiment, 75 to 80% of the total observed potential change had taken place before the corrosion rate had changed by 10%. The significance of this lag is not clear.

3.5.10.3 At the end of two hours injection of 50 ppm $NaAsO_2$ a corrosion rate of the order of 2% of the original had resulted, and was constant. After measuring the zero-impressed-current values (See Table V), cathodic polarization was carried out without much difficulty, in contrast to the trouble encountered with chromate and ferrocyanide. The mixed potential cathodic polarization curve obtained is shown in Figure 18.

3.5.10.4 Application of anodic polarizing current to the electrode inhibited with 50 ppm sodium arsenite resulted in the same general type of changes of potential and film resistance as had been noted with sodium ferrocyanide, but to a lesser degree. The potential behavior at impressed current greater than 0.02 ma/sq. cm. indicated that the film was displaced rapidly upon closing the circuit. This effect is shown clearly by the data Table VI below. Here the values of i_M, the total anodic current calculated from the rate of metal loss, corresponding to several values of I_x, are listed, together with the difference between these two values. This difference is equal to i_C, the local cathodic current.

TABLE VI

CATHODIC CURRENT DATA DURING ANODIC POLARIZATION
IN THE PRESENCE OF SODIUM ARSENITE

$\bar{I}_x$ (ma/cm^2)	$\bar{i}_M$ (ma/cm^2)	$\bar{i}_M - \bar{I}_x = \bar{i}_C$ (ma/cm^2)
0	0.014	0.014
0.010	0.025	0.015
0.040	0.064	0.024

As pointed out in Section 3.1.4, i_C should decrease as I_x (anodic) increases on a surface which is not basically altered by the passage of current. The fact that i_C actually increased in the case in question can only mean that the surface was losing the adsorbed film.

3.5.10.5 In view of this effect, it was felt that potential and resistance measurements in the presence of impressed anodic current would have little meaning. As a matter of interest, however, the potentials were measured at a limited number of points, using Procedure C to insure the minimum exposure of the film to the degrading action of polarizing current. This mixed potential data is shown as small triangles on Figure 18. The shaded area shown above the measured data points represents a "best estimate" of the region that the curve might occupy if the inhibitor film had been completely stable.

3.5.10.6 Local cell polarization diagrams for sodium arsenite are shown in Figures 21 and 23. The curves were derived from the data of Figure 18, using the procedure described in Section 3.5.4 to calculate local cell currents. In Figure 23, the local cell anode characteristic is shown as a region rather than as a line, to take into account the uncertainty of the measurements. The significance of these diagrams are discussed in Part 4 of this report.

3.5.11 Results with Long-Chain Amines

3.5.11.1 Long-chain amines are widely used as corrosion inhibitors in mildly acidic solutions. Nitrogen atoms with unshared pairs of electrons are strongly adsorbed on steel, leaving the hydrocarbon group oriented toward the corrosive medium. The resultant adsorbed film is known to prevent

a high impedance to the flow of corrosion current, but little is known about the effect of the film on the local half-cell electrode potentials themselves. Local cell polarization diagrams for amines would shed light on this and other points of the mechanism by which these inhibitors function.

3.5.11.2 Dilute solutions of the acetic acid salts of certain long-chain amines in isopropyl alcohol were found to form clear mixtures with the 3% brine at amine concentrations below 100 ppm in the brine. The amines in this category that were tested were N-oleoyl diethylene triamine, N-oleyl piperazine, and 1-(2-aminoethyl) - 2 - heptadecenyl imidazoline. The overall behavior of each of these was quite similar under the test conditions. At a concentration of 100 ppm active, each gave between 92 and 96 percent inhibition from alcohol solution. Zero-impressed-current data for a representative run using the imidazoline is given in Line 4 of Table V.

3.5.11.3 The cathodic polarization curves made on electrodes inhibited by each of these three amine salts were much alike, and so the curve for only one is shown as an illustration. A representative mixed potential cathodic polarization curve for the imidazoline injected at 100 ppm from an alcohol solution is shown as the upper curve in Figure 19. The curve appears to be a straight line at higher values of impressed current (i.e., above 0.05 ma/sq. cm.), and has no point of inflection such as is evident for the uninhibited surface.

3.5.11.4 The lower curve of Figure 19, is for the same amine salt injected at the same active concentration in diesel oil as the solvent rather than

isopropyl alcohol. The oil solution dispersed itself in the form of very small droplets with the aid of the mechanical stirrer. The inhibiting action was slower than that of the alcohol solution but after three hours 96% inhibition was observed. The curves are similar in appearance, the one for the oil solution being somewhat steeper in slope at higher values of impressed current.

3.5.11.5 Anodic polarization of surfaces inhibited with these amines gave poor results. In each case the potential began to drift in the anodic direction immediately after its initial cathodic shift following application of polarizing current. The interface resistance decreased and the interface capacitance increased during the anodic drift of potential, indicating that the inhibitor film was being removed by the action of impressed current.

3.5.11.6 Results from several runs involving the same amine salt but different degrees of inhibition in the range from 90 to 99% showed that the film on more highly inhibited surfaces was more resistant to removal by anodic current when $I_x < 10(i_C)_{I_x=0}$, but was still disrupted rapidly at currents greater than this. The film produced by the oil solution of the imidazoline also appeared to be more tenacious than that produced by an alcohol solution of this amine. For this reason an electrode treated with a diesel oil solution was chosen to supply the only consistent anodic polarization data for amine-type inhibitors that was obtained. An effort was made to measure the potential at just two points, as specified in Section 3.5.9.5. The potential was highly erratic during these measurements. Best figures for the two potential displacements were

(1) at $I_x = 10(i_C)_{I_x=0}$, 40 to 60 mv; and (2) at $I_x = 100(i_C)_{I_x=0}$, 80 to 110 mv.

3.5.11.7 The dotted curves in the upper portion of Figure 19 bound the mixed potential anodic polarization region for the surface inhibited by an oil solution of the substituted imidazoline. The point corresponding to $i_C = 0$, lies off-scale to the right of the plot shown in Figure 19, at $\log I_x = 0.4$.

3.5.11.8 Figure 21 shows the local cell polarization diagram for the imidazoline plus oil, derived from Figure 19. The local cell diagram for the other amines would appear much the same. The expanded diagram is shown in Figure 24. The shaded area between the dotted lines indicates the uncertainty in the position of the local anode curve.

3.5.12 Results with a Sulfur-Containing Organic Inhibitor

3.5.12.1 Thiourea and its derivatives are known inhibitors for acid corrosion of steel. It had been found that heating thiourea with formaldehyde under certain conditions improved the effectiveness of the parent compound[1]. This type of inhibitor was of interest to the present study because of the possibility of chemisorption by means of the sulfur groups in the molecule.

3.5.12.2 A relatively rapid decrease in corrosion rate was observed after beginning to inject 50 ppm of a condensation product prepared from

---

(1) Proprietary formulations developed by Magna Products, Inc.

one part thiourea and five parts of 34% formaldehyde solution. The corrosion rate was again constant at something less than 5% of its original value within one hour after injection had been begun. Data from a typical run with this substance is given in Table V.

3.5.12.3 The behavior of the inhibited surface toward polarizing current was quite similar to that of the electrode inhibited with sodium arsenite. Cathodic polarization was carried out without difficulty, whereas anodic polarization gave evidence that the film was being broken down, although more slowly than was the case with the other organic compounds tested. The mixed potential curves are shown in Figure 20.

3.5.12.4 The cathodic polarization branch (lower curve) shows little or no horizontal portion at lower values of I_x, and appears quite straight at higher values of I_x. The point shown as "$i_A = 0$" was located by estimation rather than by direct measurement (See Section 3.5.4), using the relationship

$$(I_x)_{i_A=0} = 2(i_A)_{I_x=0}$$

found for the uninhibited surface. It is quite certain that the multiplying factor to be used in the above equation lies between 1.5 and 2.5.

3.5.12.5 The region of most probable values for the mixed potential during anodic polarization is shown as a shaded area in Figure 20. It can be seen that the shape and position of this region for this particular inhibitor are quite similar to those of other inhibitors tested.

3.5.12.6 Local cell polarization diagrams for the thiourea-folmaldehyde condensation product, as derived from Figure 20, are shown in Figure 21, and in expanded form in Figure 25. The curve for the local anode potential is very close to a straight line, while the cathode line appears as a gentle curve. These diagrams are discussed in Part 4,

PART 4. DISCUSSION

4.1 Analysis of Results from Use of the Pearson-Holler Bridge Circuit

4.1.1 The relatively large disturbances observed to occur at the interface after sudden shifts in the DC polarizing current (required by the method of balancing the Pearson-Holler bridge) were unexpected, inasmuch as no such behavior had been reported by other workers who have used this technique (Refs. 13 and 14). Cross and Hackerman did state that "The bridge was too unstable to permit one blank run for all comparisons," but this remark was made to indicate that the shape and/or position of the polarization curves were not reproducible, rather than to point to erratic behavior during the balancing operation.

4.1.2 The disturbance was quite small at small values of applied current, but at the same time the IR drops were relatively small in this region, so no close balance of the bridge was necessary. The largest disturbances were observed in the region of greatest interest - that where the local cell current was at or near zero. Reference to Figure 13 (obtained by means of the A.C. - D.C. impedance bridge) shows why this was so. Note that both R_f and R_{D_L} changed most rapidly in the region of I_x on either side of the point where $i_A = 0$. When R_f varies with I_x, the expression for the change in bridge output due to a change in I_x (See Appendix B) contains the term

$$I_x \left(\frac{dR_f}{dI_x} \right) \Delta I_x$$

which is not present when R_f is a constant. Hence, when the rate of change of R_f with I_x is such as is shown in Figure 10B, the above term can become the major source of bridge output, obscuring the true resistive balance point

entirely. Why Cross and Hackerman (Ref. 13) and Simmons (Ref. 14) did not report similar behavior is not known. It may be that at the lower temperatures at which these workers carried out their tests the rate of change with respect to applied current was very small, or occurred very slowly and therefore did not interfere with the bridge balancing operation.

4.1.3 All known methods for obtaining a resistive balance in bridge circuits containing both resistances and EMFs depend for their effectiveness on the assumption that all the resistive elements are constant with respect to changes in current. Indeed, one primary reason for using a bridge circuit at all is to permit automatic cancellation of IR drops regardless of changes in bridge current. The fact that R_f was not constant under the conditions of the present work would therefore appear to negate the usefulness of this entire approach where changes in D.C. must be used for adjusting the resistance balance.

4.2 Polarization Behavior - Non-inhibited Surfaces

4.2.1 Cathodic Polarization - Figure 10A shows that the reduced mixed potential, PD_L, was constant at all values of I_x up to that required to reduce i_A to zero. Equations 4 and 5 (Section 1.4) indicate that for PD_L to be constant, either (a) E_A, R_A, E_C, and R_C are all constant, or (b) these same four variables change in such a manner as to leave PD_L constant. Alternative (b) is highly improbable, and is rejected in favor of (a). Constant values for the E's and R's imply constant true anodic current density and true cathodic current density (See Footnote, Section 1.1). This analysis leads to the conclusion that the size of the true anodic and cathodic areas must change with the applied current in such a manner as to leave the

respective current densities essentially constant. When the applied current is cathodic, as in Figure 10, the total area undergoing anodic local cell action becomes smaller as I_x is increased up to $(I_x)_{i_A=0}$. As I_x approaches $(I_x)_{i_A=0}$, the number of anodic sites becomes relatively small and the distribution probably is non-uniform. Under these conditions the simple relationship expressed by Equation 4 probably no longer applies.

4.2.2 The theoretical relationship of potential to polarizing current for activation-controlled electrode processes has been treated by Stern (Refs. 28 to 32). It is shown that no change in the "potential" is to be expected even on a cathode of constant area until the impressed current becomes about equal to the original local cell current. Stern does not define his "potential," however, and it is not known whether he is referring to PD_L or PD_p. It is probable that the corrosion reaction studied here is subject to control by both activation (for the hydrogen half-reaction) and diffusion. Thus, the potential behavior may be expected to be complex and difficult to analyze.

4.2.3 A contributing cause for the more rapid change of potential in the region of zero local cell current may be found in the dependence of mixed potential on the ratio of anodic areas to areas on the electrode surface (Ref. 33). Figure 8 of Reference 33 shows that, for electrodes that exhibit Tafel behavior, the potential moves sharply in the anodic direction when A_C/A_A becomes very small. Here again, the mathematical analysis applies strictly only to "perfect" electrodes, but helps to understand the overall behavior of the real electrode.

4.2.4 Both PD_L and PD_P show a point of inflection at or near where $i_A = 0$. It is apparent that the current corresponding to this inflection could be used to determine the value of I_x corresponding to $i_A = 0$. The relationship between this value of I_x and the original (maximum) value of i_A (equal to the local cell corrosion current) cannot be determined from the polarization diagram, however. The ratio of $(I_x)_{i_A=0}$ to $(i_A)_{max.}$ (as measured at $I_x = 0$) varied from 1.5 to 2.5 for several uninhibited runs. A possible reason for such variation may be found in Equation A-4 of Appendix A:

$$i_A = i_L \pm I_x\left(\frac{R_C}{R_A + R_C}\right) \qquad \text{(Equation A-4)}$$

This equation shows that the fraction of I_x that affects i_A is determined by the ratio $R_C / (R_A + R_C)$ at any instant. If this ratio is different from one run to another, then i_A will be a different function of I_x accordingly. If i_A in Equation A-4 is set equal to zero, then we have

$$(I_x)_{i_A=0} = \pm (i_L)_{i_A=0} \cdot \left(\frac{R_A + R_C}{R_C}\right)_{i_A=0} \qquad \text{(Equation 16)}$$

Substituting for i_L from Equation 5, Section 1.4:

$$(I_x)_{i_A=0} = \pm\left(\frac{E_A - E_C}{R_C}\right)_{i_A=0} \qquad \text{(Equation 17)}$$

Of the three quantities on the right of Equation 17, $(E_A)_{i_A=0}$ and $(R_C)_{i_A=0}$ have been determined as -0.875 v. vs. SCE and 30 ohms/cm^2 respectively, but $(E_C)_{i_A=0}$ cannot be measured on a mixed electrode.

4.2.5 The curve for R_f vs. I_x shown in Figures 10B and 11B lends support to the view that local anodes areas are converted to cathodic areas by the applied current. As shown by Equation 7, R_f is equal to the parallel combination of R_A and R_C, the local anode and cathode resistances:

$$R_f = \frac{R_A \cdot R_C}{R_A + R_C} \qquad \text{(Equation 7)}$$

R_A and R_C are the result of all individual anodes, or cathodes, acting in parallel. Thus, each is inversely proportional to the areas acting as anodes or cathodes, respectively. As the area acting anodically is decreased by increasing I_x, $\bar{R}_A$ increases greatly, while $\bar{R}_C$ decreases only slightly, in line with the concept that the steel surface has a high ratio of cathodic to anodic areas in acid solutions. The net result is an increase in $\bar{R}_f$. Figure 10B shows that $\bar{R}_f$ increases by a factor of three from the initial state to the point where $i_A = 0$. Beyond this point the surface is entirely cathodic, and $\bar{R}_f$ is seen to decrease with increasing I_x, presumably because previously inactive areas on the surface are thereby brought into play. This statement is supported by the increase in the interface capacitance $\bar{C}_f$ which occurs at higher values of I_x (See Figures 10B and 11B).

4.2.6 Two distinct differences appear between the curves of Figure 10 obtained by means of Polarization Procedure A, and Figure 11 obtained by means of Polarization Procedure B. One is that, in Figure 10A, the potential curves are flatter at low values of I_x and break more suddenly. The other difference is the sharpness and symmetry of the peak in the curve for $\bar{R}_f$ in Figure 10B as compared to the broader curve screwed to the left in Figure 11B. The curves of Figure 10 are believed to represent somewhat

better data than those of Figure 11, inasmuch as each point in the former diagram was measured relative to a zero-impressed-current value taken immediately before the said point. Thus, any off-set of the zero value was taken into account. This was not true of the data shown in Figure 11, where the impressed current was increased from point to point without returning to zero. However, from a practical point of view, it appears that the possible errors introduced by use of Procedure B on the uninhibited surface are small in comparison to the effects to be expected from inhibitors in the solution, and hence, when the polarization curve is measured only to serve as the starting point for a study of inhibitors, Procedure B is preferred for the saving of time it allows.

4.2.7 Figures 13 and 14 show the local anode polarization curves corresponding to data obtained by Polarization Procedures A and B, respectively, for the uninhibited surface. Along the X-axis is plotted the ratio of the anodic local cell current, (i_A), to its maximum value, measured when $I_x = 0$. The magnitude of the abcissa is directly proportional to the average rate of corrosion over the electrode surface. No assumptions need be made regarding the area actually undergoing anodic reaction. In the absence of methods to determine the true local anode current density, it is believed that this method of presenting of local cell polarization curves is the most generally useful of several methods appearing in the literature.

4.2.8 As shown in Figure 13, the total polarization of the local anode potential under the test conditions is considerable - totalling 150 mv. as measured by Procedure A. Seventy-five percent of the total occurs over

only 25% of the range of i_A near $i_A = 0$. Thus, unless the entire polarization curve is traced, the relatively wide region over which the potential is constant can give the mistaken impression that the anodic reaction is only slightly polarized.

4.2.9 The so-called "open circuit" anode potential is seen to be -0.875 v. vs. SCE. No fundamental significance is attached to this value, except to note that it was measured when i_A was zero and when no dissolved iron was present in the solution. Some concentration of ferrous ion other than zero may persist near the metal surface as an adsorbed layer or as a layer of solution trapped by the hydrogen gas blanket generated by the cathodic polarizing current. The iron electrode is essentially irreversible in this solution, and so the Nernst Equation is of no value in making the analysis.

4.2.10 Anodic Polarization - Figure 15 shows data obtained by anodic polarization of the uninhibited steel electrode under the test conditions. These curves represent the behavior in the region of I_x extending from near zero to about 25% of the current required to reduce i_C to zero. Originally it was planned to supply enough anodic polarizing current to reach the point where $i_C = 0$, but the amount of applied current required proved to be far greater than expected, and so the total change in i_C produced was limited by practical considerations of equipment available and circuit design. The portion of the polarization curve that was accessible is of considerable value, nevertheless, for making comparisons with anodic polarization data obtained when inhibitors were applied.

4.2.11 If the behavior of the surface toward anodic polarization current were strictly analogous to that toward cathodic current, the slope of the line

for PD_L would be close to zero over the entire region shown on Figure 15A. The continuous decrease of $\bar{R}_f$ shown in Figure 15B indicates that cathodic areas are being converted to anodic areas to a certain extent as I_x increases. The shift of PD_L, and along with it PD_p, in the cathodic direction probably results from the fact that there is considerable resistance to the conversion process, and hence new anodic areas are not created in proportion to increasing anodic current. Therefore, the true anodic current density increases and the true cathodic current density decreases as anodic impresses current increases, resulting in a net shift of both potentials in the cathodic direction.

4.2.12 The local cathode polarization curve for the uninhibited steel electrode, shown in Figure 17, is quite different in appearance from the local anode curve of Figure 13. (Both curves are shown together in Figure 26 for more convenient comparison). The curvature of the cathodic curve is more or less constant throughout its length, and the slope is steeper than that of the anodic branch, commensurate with the greater total change of potential of 0.43 v. as compared to 0.15 v. for the total anode shift. Note that both curves have nearly the same slope during the first 10% of the maximum local cell current, but that from that point on the local cathodic curve has a much greater slope than the anode curve.

4.2.13 The best estimate of the open circuit cathode potential obtainable from the extrapolated local cathode curve is -0.300 v. vs. SCE. This is the same as that of the standard hydrogen electrode, but probably only by coincidence. The surface is presumably behaving as a hydrogen electrode at

equilibrium when $i_C = 0$ (in addition to the highly polarized anodic activity taking place), and therefore if the Nernst Equation for this half-reaction (Equation 18) applies, the observed potential indicates that the activity of hydrogen gas at

$$E_H = \frac{RT}{nF} \log \frac{(H^+)^2}{(H_2)} \qquad \text{(Equation 18)}$$

the interface was approximately equal to the square of the hydrogen ion activity, or about 10^{-9} M. The sweeping effect of moving solution and CO_2 bubbles should maintain the partial pressure of H_2 very low, especially when $i_C = 0$ and no hydrogen is being generated.

4.2.14 The main use to be made of $(E_C)_{i_C=0}$, or $(PD_C)_{i_C=0}$ in Figure 17, is as a reference point from which to measure the effect of inhibitors in shifting the open circuit cathode potential. As described in Section 3.5, the changes in this value caused by most good inhibitors was of the order of 200 mv., and hence the uncertainty of 50 mv. in $(E_C)_{i_C=0}$ does not greatly interfere with interpretation of the data.

4.2.15 At the outset of this work, it was hoped that, once the local cell polarization potential curves had been obtained, they could be resolved into two components, one electromotive and the other resistive, in accordance with Equations 1 and 2, Section 1.2. Such a resolution would depend on being able to measure or estimate R_A and R_C at any point. Unfortunately, it was not possible to measure these values separately; only their parallel combination R_f could be determined.

4.2.16 Some idea of the order of magnitude of the resistance per unit area of actual anodic area or of actual cathodic area may be derived from the

respective values of R_f when i_C or i_A, respectively, are equal to zero. Thus, from Figure 10A, $\bar{R}_f$ equals 30 ohms per sq. cm. apparent at the point where local anodic activity is stopped and the surface presumably is acting entirely as a cathode with about the same fraction of the total available surface being utilized as when i_A was not zero. Thus, the approximation would be $(\bar{R}_C)_{i_A=0} \cong (\bar{R}_f)_{i_A=0} = 30$ ohms per apparent sq. cm. Similarly, Figure 15A shows that $\bar{R}_f$ approaches 2 ohms per apparent sq. cm. as i_C approaches zero. Therefore, $(\bar{R}_A)_{i_C=0} \cong (\bar{R}_f)_{i_C=0} = 2$ ohms per apparent sq. cm. These must be regarded as degenerate values, considering the special conditions under which they apply. Furthermore, because they are resistances per unit of area, they cannot be used to calculate the effective values of R_A and R_C because the respective areas actively engaged in transferring current to the solution were not known or measurable.

4.2.17 A further complication in the scheme to resolve polarization curves into EMF and resistance terms is introduced by the variation in R_f, and thus of R_A and R_C, produced by varying the impressed current. If R_A or R_C were constant over the entire region of local cell current, then certain assumptions might be made and the straight line that would correspond to the term $i_A R_A$ or $i_C R_C$ might be drawn on the diagrams. As it is, this method can be suggested but cannot be used.

4.2.18 The curve for PD_A appears to be close to that which can be described by a Tafel-type equation. Using the general form of the equation:

$$PD_A = a + b \log i_A \qquad \text{(Equation 19)}$$

and setting a = -0.88 v. (corresponding to $i_A = 0$) and b = +0.50 (calculated using only the two end-points of the measured potential curve), a curve indicated by the position of the small crosses in Figure 13 is obtained. The two curves might be said to coincide within the normal amount of variation in potentials measured from one run to another. This would be a significant observation were it not for several complicating factors. First, in the Tafel Equation the symbol "i" in the log i term refers to the true current density, and thus if the total current is used as a variable, it must be assumed that the area receiving that current is constant. But on the mixed electrode being studied here, several indications point to local anode area which decreases with i_A in such a manner that the true anodic current density is relatively constant. If such is actually the case, and Equation 19 does in fact apply, then only a small change in the local anodic potential should have occurred as i_A was reduced. It is apparent that too many unmeasured variables are operating during polarization by impressed cathodic current to permit a detailed analysis of the behavior. The same remark applies also to polarization occurring during application of anodic current. Therefore, as stated previously, the primary usefulness of the local cell polarization curves to the present study is as a qualitative comparison by which the effect of inhibitors may be judged.

4.3 Analysis of Zero-Impressed-Current Potential Data for Inhibited Surfaces

4.3.1 As shown in Table V, all inhibitors produced a displacement of the zero-impressed-current potential toward the cathodic (less negative) direction. Examination of Figures 22 to 25 in conjunction with Figure 25 shows that all inhibitors tested moved the open-circuit potential of local anodes in the cathodic direction by at least 100 mv. and some moved it

over 200 mv. In addition, the equilibrium mixed potential in the presence of inhibitors was in every case at least 60 mv. more cathodic than the open-circuit anode potential. Thus, the sum of these two displacements was greater than 160 mv., which placed the inhibited mixed potentials at more cathodic values than the uninhibited mixed potentials. In most cases even the open-circuit local anode potential of the inhibited surface was more cathodic than the polarized mixed potential of the uninhibited surface. See, for example, Figures 23, 24, and 25.

4.3.2 The total displacement of mixed potential for each of the six inhibitor runs tabulated in Table V is given in Table VII.

TABLE VII

ZERO-IMPRESSED-CURRENT POTENTIALS SHIFTS FROM TABLE V

INHIBITOR	POTENTIAL CHANGE (mv.)
Sodium Chromate	57
Sodium Ferrocyanide	38
Sodium Arsenite	70
Alkyl Imidazoline	102
Alkyl Imidazoline plus Oil	107
Thiourea Derivative	92

As shown, the organic chemicals gave larger potential changes than did the inorganic chemicals at the particular concentrations indicated in Table V. However, potential displacement increased with increasing concentration of inhibitor in all cases, so that the relative order of displacements was

somewhat different depending on the concentration in the solution at the time the potential was measured. For example, one run involving sodium arsenite at 70 ppm gave a shift of over 100 mv. at 99.5% inhibition.

4.3.3 The potential appeared to be more sensitive to the concentration of inhibitor in the solution than to the degree of film formation indicated by the corrosion rate. As described in Section 3.5.8.2 for sodium arsenite, the potential began to change immediately after starting to inject the inhibitor, even through the corrosion rate often required 15 to 30 minutes to begin to change. This effect occurred in reverse after a constant inhibited state had been reached. As soon as the supply of inhibitor was cut off, the potential began to move toward more anodic values, and yet the corrosion rate remained constant for some time.

4.3.4 Two experiments were carried out to examine this phenomenon further. In one, the system was inhibited with sodium arsenite, and after a constant inhibited potential had been measured, the inhibitor was shut off and the flow of solution was allowed to continue for 16 hours. At the end of that time, the percent inhibition had decreased only from 98 to 82%, but the potential was actually more anodic than it was before the inhibitor had been injected. The other experiment involved the oil solution of the alkyl-imidazoline salt. The system was first inhibited 98%, maintained there by continuous injection for four hours, then allowed to go for sixteen hours without inhibitor. Inhibition was still at 97% at the end of this time, indicating good persistency of the adsorbed film. The potential had returned to within 20 mv. of its original uninhibited value, nevertheless. It is apparent from these results that no correlation between the magnitude of the potential shift and the effectiveness of an inhibitor is to be expected.

4.4 Effect of Inhibitors on Interface Resistance and Capacitance

4.4.1 It is of interest to compare the change in the interface resistance and in the interface capacitance produced by each inhibitor, with the corresponding change in corrosion rate. Table VIII gives the percent change in conductance ($1/\bar{R}_f$), capacitance ($\bar{C}_f$), and in corrosion rate for the data shown in Table V.

TABLE VIII

INTERFACE CONDUCTANCE AND CAPACITANCE DATA

INHIBITOR	% DECREASE IN $1/\bar{R}_f$	% DECREASE IN $\bar{C}_f$	% DECREASE IN CORROSION RATE
Sodium Chromate	72	78	85
Sodium Ferrocyanide	84	31	95
Sodium Arsenite	96	79	98
Alkyl Imidazoline	90	44	93
Alkyl Imidazoline plus Oil	89	74	98
Thiourea Derivative	90	64	95

4.4.2 R_f is a measure of R_A and R_C in parallel, whereas R_A and R_C are in series in the path of local cell corrosion current. If R_A and R_C are both increased by the same factor by the action of an inhibitor, then R_f would increase by this same factor and changes in R_f would correctly indicate changes in $R_A + R_C$. However, if an inhibitor has an unequal effect on R_A and R_C, then R_f will change in an unpredictable manner. It is regrettable that no method was found to measure R_A and R_C separately on the mixed electrode.

4.4.3 No direct correlation is to be expected between either R_f or the sum of R_A and R_C and the corrosion rate, inasmuch as the local cell current is a function both of local half-cell resistance and local half-cell EMF's, as shown in Equation 5, Section 1.4. A study of Table IX reveals that changes in the EMF relationships produced by inhibitors were considerable, and appeared to have an effect on the corrosion rate that was comparable to that of the cell resistances.

4.4.4 The figures for interface capacitance are listed in Table VIII as a matter of interest. The interpretation of the capacitive reactance of an electrode interface is still on open question. Simmons (Ref. 14) contends that no true capacitance exists, and instead only an apparent capacitive effect exists because changes of potential lag behind changes in current across the interface. On the other hand most workers in the field of hydrogen overvoltage talk about an electrical double layer across which electrical charge can be transferred rapidly. It is not the purpose of the present work to attempt to resolve these fundamental matters. The capacitance, apparent or otherwise, was measured to indicate the degree to which the layer of charged molecules originally adsorbed on the steel had been displaced by each inhibitor. From the data of Table VIII there appears to be only a rough qualitative correlation between the decrease of C_f and the decrease in local cell corrosion.

4.4.5 Table VIII shows that the imidazoline injected from an alcohol solution into the brine in the absence of oil produced a 90% increase in film resistance and a 93% reduction in corrosion. Simmons (Ref. 14) reported

that certain water soluble inhibitors, presumably amine salts, give essentially no increase in "film resistance" in his tests. It is possible that he did not take into account the slow rate of adsorption of this class of compounds at low concentrations, and thus did not wait long enough for the adsorbed layer to be established. Simmons did find a strong effect of oil solutions of amine inhibitors, and thus concluded that there might be a fundamental difference between the mechanism of inhibition depending on whether oil was present or absent. The results of the present work show, however, that the amines are strongly adsorbed from both water and oil solutions, and that the role of oil is probably one of adherence to the "tails" of the adsorbed molecules in such a manner as to further increase the resistance of the film to penetration by water, hydronium ions, ferrous ions, and other species involved in the corrosion reaction.

4.5 Local Cell Polarization Diagrams for Inhibitors

4.5.1 Comparison of the four local cell polarization diagrams of Figures 22 through 25 with each other shows that the observed polarization behavior was very much the same regardless of the inhibitor used. Because of this similarity, the different inhibitors will be discussed together under headings that refer to the behavior of the inhibitors as a group.

4.5.2 Open-circuit Potentials. Table IX gives a compilation potential data for the four inhibitors for which complete local cell data is available. The values shown for $(E_A)_o$ are probably all more cathodic (less negative) than they should be, due to the effect of cathodic polarizing current in increasing the adsorption of inhibitors during the experimental procedure. For sodium ferrocyanide, the effect may be due to precipitation of unsoluble

TABLE IX

LOCAL CELL POTENTIAL DATA FOR INHIBITORS

INHIBITOR	EQUILIBRIUM MIXED POTENTIAL (mv. vs SCE)	OPEN-CIRCUIT ANODE POTENTIAL $(E_A)_o$	OPEN-CIRCUIT CATHODE POTENTIAL $(E_C)_o$	$(E_C)_o - (E_A)_o$ (mv.)
Sodium Ferrocyanide	-675	-735 to -775	-605 to -575	130 to 200
Sodium Arsenite	-652	-722	-572 to -542	150 to 180
Imidazoline	-615	-688	-535 to -495	160 to 190
Thiourea Derivative	-632	-682	-557 to -532	130 to 150

iron compounds closer to the metal surface of anode areas made possible by decreasing anodic current. For sodium arsenite, the chemical reducing action of cathodic current could cause an accelerated deposition of arsenic in close proximity to local anodes, tending to choke them off more than was the case before the polarizing current was applied. For the organic compounds, which presumably act primarily by physical adsorption without chemical change, increased adsorption at anodic areas could result from the increased rate of transport of positive ions to the surface under the applied potential gradient, such positive ions including those from ionization of amines and oxonium compounds in the acid solution. No definite figure can be placed on the magnitude of the error introduced by this phenomenon, but it probably is less than 50 mv. in all cases. No similar statement may be made for the values of $(E_C)_D$, because no stable measurements could be made, as described previously. The values shown have already been "corrected" for the fact that the protective film was partially destroyed by the anodic current.

4.5.3 Recall that the values for $(E_A)_D$ and $(E_C)_D$ on the uninhibited surface were -880 and -300 mv. respectively. Thus, the open circuit local anode potentials were shifted in the cathodic direction by something between 100 and 200 mv. by the inhibitors examined. Likewise, the open circuit cathode potentials were shifted anywhere between 200 and 300 mv. in the anodic direction. The fact that any shift in open-circuit potentials occurred at all is of considerable interest, inasmuch as there appears to be common tendency to draw local cell polarization diagrams for inhibitors in such a way that no change in open-circuit potentials is shown. Such diagrams are, of course, very often drawn with little if any experimental data to support them.

4.5.4 There is some justification for the assumption that the open circuit potentials of local cells remain roughly constant in the presence of an inhibitor during the early stages of film formation. The viewpoint may be taken that the formation of an adsorbed inhibitor film serves to inactivate that portion of the surface on which the film is adsorbed, but leaves the remaining area the same as before. In other words, the electrode area is reduced but not otherwise altered. Thus, as long as the electrochemical properties of the remaining areas are the same as before, the corresponding open circuit potentials would presumably remain unchanged. However, as film coverage becomes more and more complete, the metal is exposed to the solution only through small pores. Under these circumstances, the concentration of ions affecting the electrode potential of different areas ceases to bear any direct relation to the concentrations in the bulk of the solution. Products of the corrosion reactions such as ferrous ion and hydrogen gas are trapped in the pores; thus, the open circuit potential of local anodes becomes more cathodic and that of the local cathodes becomes more anodic.

4.5.5 It may be seen from Table IX that the difference between the open circuit potentials of local anodes and cathodes varied between 130 and 200 millivolts for all inhibitors tested. This may be compared to the open circuit potential difference of 580 millivolts for the uninhibited surface. Thus, the inhibitors reduced the open circuit potential difference upon the surface to about 1/3 of its original value. Consequently, a corresponding reduction in the local cell corrosion rate may be accounted for without any increase in the slope of the local anode and local cathode polarization curves. However, the remainder of the observed inhibitor effectiveness was accounted for by an increase of the slope of these curves. This affect is discussed below.

4.6 Polarization Resistance

4.6.1 All local cell polarization curves appear to be curved to some extent. Thus, it is not meaningful to refer to any one of these as having a single slope. However, for the purpose of analysis each curve may be assigned an "average polarization resistance" which is defined as the total change of local half-cell potential from one end of the curve to the other, divided by the maximum local cell current associated with that curve. This concept of average polarization resistance has utility in connection with local cell curves because only the end points of these curves have practical significance in the interpretation of inhibitor behavior.

4.6.2 Table X shows the values of the average polarization resistance for the anode and cathode branches of local cell polarization diagrams for the uninhibited electrode and the electrode inhibited with the four inhibitors for which local cell diagrams are presented in Figures 22 through 25.

TABLE X

AVERAGE POLARIZATION RESISTANCE - (APR) FOR INHIBITORS

INHIBITOR	"APR" ANODIC (ohms/cm^2)	"APR" CATHODIC (ohms/cm^2)
None	150	400
Sodium Ferrocyanide	1000	1000
Sodium Arsenite	2800	4000
Subst. Imidazoline	1500	2000
Thiourea Derivative	1500	3000

Note first of all that the polarization resistance calculated for uninhibited local anodes is roughly 100 times the interface resistance of anode areas estimated as discussed in Section 4.2.16. The polarization resistance shown for local cathodes is roughly ten times the interface resistance for cathodes estimated from alternating current measurements. Thus, if the values determined by alternating current measurement are assumed to be essentially correct for the true resistive component of the total polarization, it is apparent that this component contributes such a small affect to the total change in potential that it may be neglected without much error.

4.6.3 Polarization resistance figures shown for inhibited surfaces are also of the order of ten or more times greater than interface resistances found on inhibited surfaces. Here again, it appears that the purely resistive component of total polarization accounts for only 10% of the observed change in potential, even though the resistive component increases considerably in the presence of an effective inhibitor.

4.6.4 The variation in polarization resistance resulting from the action of the four inhibitors tested was much greater than the variation observed in the open circuit local cell potentials produced by these inhibitors. Thus, the main source of difference between inhibitors was found in the average polarization resistance. These differences show clearly in Figure 21 where each of the diagrams is drawn to the same corrosion current scale. Although these differences in polarization resistance are interesting, they probably should not be used to draw conclusions about basic differences in the inhibitor film unless the data apply to measurements made at the

same degree of inhibition. In clarification of this point, note from Figure 21 that sodium ferrocyanide showed the poorest inhibition and sodium arsenite the best inhibition; and at the same time Table X shows that sodium ferrocyanide had the lowest polarization resistance on both anodes and cathodes, whereas, sodium arsenite had the highest polarization resistance. Thus, it appears that polarization resistance (as defined in Section 4.6.1) is more a function of the degree to which film formation by an inhibitor is completed than it is of the type of inhibitor involved. Unfortunately, the exact amount of residual corrosion was difficult to control in the presence of the inhibitors tested. Thus, a comparable set of polarization diagrams measured starting from the same inhibited corrosion current for each of the four inhibitors was not available.

4.6.5 The results discussed above may be interpreted in terms of a mechanism of corrosion inhibition which involves adsorption of a protective layer to an approximately equal extent on both local anodes and local cathodes of the mixed corroding electrode. Although the data indicates a somewhat stronger overall effect on cathodes, polarization resistance at local anodes was increased more than was that at cathode areas by the action of inhibitors. The fact that the film resistance was responsible for such a small fraction of the total observed polarization for these inhibitors indicates that the primary mode of action is a plastering effect by which most of the original active area is inactivated and transference of ions and molecules through residual pores in the protective layer is highly

impeded. The similarity in the polarization diagrams of the four inhibitors examined tends to show that the protective layer in each case was rather inert; that is, it did not take part in any electrochemical reaction itself. Such inertness was expected for the film deposited by sodium ferrocyanide, the amine and the thiourea derivative. For sodium arsenite, however, it was thought that a large area of deposited arsenic might act as cathode for a few small remaining anode areas, thus promoting a pitting action where film formation was not complete. This question appears to have been answered negatively by the very high value of polarization resistance determined from the cathodic branch of the local cell diagram for sodium arsenite.

4.6.6 Throughout this discussion it has been tacitly assumed that the percentage of corrosion inhibition was a direct measure of the percent of the surface covered by the protective film. As a matter of fact, however, no such correlation was established. At the outset of this work, it was hoped that the interface capacitance might prove to be some measure of the electrochemically active area on the metal surface. Simmons (Ref. 14) and others have shown that adsorption of inhibitor films causes a very large decrease in the interface capacitance as might be expected from the displacement of the electrochemical double layer along with the water adsorbed at the metal surface. As has been pointed out in Section 4.4, Table VIII shows that there was very little correlation between the decrease

in the interface capacitance and the decrease in corrosion rate for the various inhibitors tested. Whether the measured value of the interface capacitance was not proportional to the residual active areas, or whether the corrosion current was not proportional to the residual areas is not known. Thus, little directly useful information bearing on the true current density at local anodes and cathodes in the presence of inhibitors was obtained from this work.

4.6.7 It may be noted that data for the reduced potential, PD_L, has been omitted from all polarization diagrams for inhibitors. This was done because the difference between the curve for PD_L and that for PD_P was less than 5 mv. at any point over the range of I_x that was of interest, and this difference was never enough to give the curve for PD_L any distinctive features. As pointed out in Section 1.11, local cell polarization diagrams in this report were constructed from data for PD_P and not from data for PD_L. It is apparent that, for practical purposes of studying the overall effects of inhibitors and comparing one inhibitor with another on steel electrodes immersed in salt water, the IR drop due to flow of polarizing current across the interface should be included in the polarized potential. Therefore, since IR drops through salt water solutions are negligible compared to potential changes at the metal-solution interface, good, useable potential data may be obtained by direct measurement from a reference electrode located at a convenient distance from the electrode surface.

SUMMARY AND CONCLUSIONS

The following statements summarize the accomplishments and results of the work carried out under this contract.

1. In order to eliminate the effect of internal cell resistance on the electrode potential measured in the presence of polarizing current, a circuit similar to a Pearson Bridge was constructed and the technique of super position of small increments in the D.C. polarizing current was used to adjust the bridge circuit. After considerable testing, this circuit and general method was found to be unsuitable for the electrode system being studied, primarily because of high rates of change of both interface resistance and electrode potential with change of polarizing current in the region where the local cell current is close to zero.

2. A special impedance bridge was then constructed by means of which the interface resistance and the interface capacitance shunting this resistance could be measured without changing the D.C. polarizing current. This circuit was used successfully throughout the remainder of the work.

3. A relatively simple equivalent circuit was drawn up to represent the metal solution interface of the corroding electrode. All data was interpreted in terms of this equivalent circuit. It was shown that equations for the local cell polarization curves could be derived simply from the electrical analogy of the interface.

4. Local cell polarization curves for the uninhibited steel electrode were determined without difficulty with the help of a recording Corrosometer which measured corrosion continuously at all times during the runs.

The open circuit potential difference between uninhibited local anodes and cathodes as indicated by the polarization curves was 0.58 volts at pH 4.5. The slope of the local cathode curve was considerably steeper than that of the local anode curve as a result the equilibrium mixed potential was only 150 milivolts more cathodic than the open circuit anode potential.

5. Local cell polarization curves for a number of different types of inhibitors were determined. Passage of polarizing current to or from an inhibited surface produced irreversible effects at the interface causing the amount of inhibitor adsorbed to change and often obscuring the true potential behavior of the electrode. Disturbances were especially severe during anodic polarization and as a result data for inhibitors obtained under these conditions had to be extrapolated to that corresponding to a theoretical undisturbed state before it was plotted on the diagram.

6. More or less complete data was obtained for four different inhibitors representing four separate types of inhibitor compounds. These were (1) sodium ferrocyanide, (2) sodium arsenite, (3) a high-molecular-weight amine, and (4) a substituted thiourea. The local cell polarization diagrams obtained for these four inhibitors were very similar to each other, indicating that the mechanism of inhibition may be much the same for each. This mechanism appears to involve the inactivation of a large portion of the electrode area by an inert film along with a deactivation of residual areas not covered by the protective layer.

7. The shapes of all local cell polarization curves obtained in this work were complex and did not lend themselves to simple analysis in terms of the sum of a resistance term and a logarithm term representing interface resistance and activation polarization respectively. This was not suprising in view of the evidence obtained to show that anodes and cathodes were converted from one to the other by the affect of polarizing current and that both concentration polarization and diffusion effects were present.

8. A concept called "average polarization resistance" was defined as the total polarization of local cell potential divided by the maximum local cell current. Average polarization for inhibitors correlated best with the residual corrosion current associated with the inhibited state.

9. The general method of studying corrosion and corrosion inhibitors, comprising the determination of quantitative local cell polarization data, is potentially very valuable. From a practical standpoint, its use would appear to be limited by the time and effort required to obtain meaningful data, and by the instability of the metal surface toward passage of impressed current. The experimental difficulties involved may be expected to vary widely depending on the particular metal and corrosive system involved.

APPENDIX A

A Derivation of the Relationship Between the Direct Mixed Potential PD_P and the Reduced Potential PD_L

According to Equations 3 and 4 (Sections 1.3 and 1.4), PD_P and PD_L are defined as:

$$PD_P = E_A + i_A R_A \qquad \text{(Equation A-1)}$$

$$PD_L = E_A + i_L R_A \qquad \text{(Equation A-2)}$$

When no impressed current is flowing to or from the electrode surface, $i_A = i_L$, and so $PD_P = PD_L$. When an impressed current I_x is flowing, i_A will be greater or less than i_L depending on whether the impressed current is anodic or cathodic. Referring to the equivalent circuit of Figure 1, it is assumed that I_x will be distributed according to Kerchoff's Laws. Thus the fraction flowing in R_A is given by

$$(I_x)_A = I_x \cdot \left(\frac{R_C}{R_A + R_C}\right) \qquad \text{(Equation A-3)}$$

Therefore

$$i_A = i_L \pm (I_x)_A = i_L \pm I_x \cdot \left(\frac{R_C}{R_A + R_C}\right) \qquad \text{(Equation A-4)}$$

Substituting Equation A-4 for i_A in Equation A-1:

$$PD_P = E_A + \left[i_L \pm I_x \cdot \left(\frac{R_C}{R_A + R_C}\right)\right] R_A$$

$$= E_A + i_L R_A \pm I_x \cdot \left(\frac{R_A R_C}{R_A + R_C}\right) \qquad \text{(Equation A-5)}$$

Noting that the expression in parentheses is the parallel sum of R_A and R_C, which is by definition equal to the interface resistance R_f, there results

$$PD_p = E_A + i_L R_A \pm i_x R_f \qquad \text{(Equation A-6)}$$

Comparison of Equation A-6 with Equation A-2 shows that

$$PD_p = PD_L \pm I_x R_f \qquad \text{(Equation A-7)}$$

which is given as Equation 6 in the text (Section 1.6).

APPENDIX B

Analysis of Electrode Potential Behavior as Effected By Changes in Polarizing Current

Equation 11, Section 1.19 expresses the overall potential difference measured between an electrode and a reference point in the solution (See Figure 1) as:

$$PD_j = PD_L \pm I_x R_f \pm I_x R_s = PD_L \pm I_x(R_f + R_s) \qquad \text{(Equation B-1)}$$

If PD_L is to be determined, it is necessary to eliminate the effect of resistances R_f and R_s. A bridge circuit (e.g., the Pearson Bridge) may be used to accomplish this more or less automatically, provided R_f is constant with respect to changes in I_x used to adjust the bridge balance. In this case, the change in PD_j produced by a small change in I_x may be expressed as:

$$\Delta PD_j \Big|_{R_f} = \left(\frac{dPD_L}{dI_x}\right) \Delta I_x \pm (R_f + R_s)\ \Delta I_x \qquad \text{(Equation B-2)}$$

The assumption is then made that $\frac{dPD_L}{dI_x}$ is small compared to $R_f + R_s$. When this is done, the error signal obtainable from the bridge circuit becomes proportional to the difference between $R_f + R_s$ and the setting of one or more arms of the bridge, so that, at null, the contribution of the resistive term of Equation B-1 is cancelled out, leaving PD_L.

If $\frac{dPD_L}{dI_x}$ is not much smaller than $R_f + R_s$, then the balance point of a bridge will not accurately reflect the purely resistive components of the

cell. For steel in contact with brines, $\frac{dPD_L}{dI_x}$ was much larger than R_f + R_s except where $I_x < i_{corr.}$, so that changes in I_x could not be used successfully to separate the terms of Equation B-1. In such circumstances it is possible to proceed by neglecting the IR drops, as they will be small when compared to changes in PD_L. However, this does not solve the problem of measuring R_f itself.

Another source of interference that may be introduced by a change of polarizing current (I_x) arises when R_f changes with I_x. If both PD_L and R_f are considered functions of I_x, then the differential of Equation B-1 becomes:

$$\Delta PD_J = \left(\frac{dPD_L}{dI_x}\right) \Delta I_x \pm I_x \left(\frac{dR_f}{dI_x}\right) \Delta I_x \pm \Delta I_x (R_f + R_s) \quad \text{(Equation B-3)}$$

The second term of Equation B-3 is seen to contain I_x as a factor, and thus increases proportional to I_x. Thus when R_f and R_s are relatively low, their effect on ΔPD_J may be completely masked by the effect of a change in R_f.

REFERENCES

1. R. B. Mears and R. H. Brown, J. Electrochemical Soc. 97, 75 (1950).

2. A. L. Ferguson, Trans. Electrochemical Soc. 76, 113 (1939).

3. W. J. Muller, ibid, 76, 84; 167 (1939).

4. U. R. Evans, "Metallic Corrosion, Passivity, and Protection," Arnold (London) 1937.

5. (a) R. H. Brown, G. C. English, and E.D. Williams, Corrosion 6, 136 (1950).
   (b) M. Stern, Corrosion 13, 775 t (1957).

6. (a) R. H. Brown and R. B. Mears, Trans. Electrochemical Soc. 74, 495 (1938)
   (b) U. R. Evans and T. P. Hoar, Proc. Royal Soc. (London) A137, 343 (1932).

7. L. J. Benson, R. H. Brown and R. B. Mears, ibid, 75, 259 (1939).

8. R. H. Brown and R. B. Mears, Trans. Faraday Soc. 35, 467 (1939).

9. H. D. Holler, J. Electrochemical Soc. 97, 271 (1950).

10. W. R. Scott and G. H. Rohrback, Corrosion 7, 234 (1952).

11. (a) G. H. Rohrback, Paper presented at Sixth Annual Western Regional Corrosion Conf., N.A.C.E., Long Beach, Calif. Nov. 1956
    (b) D. H. Stormont, Oil and Gas Journal 55, No. 3 (1957)

12. J. M. Pearson, Trans. Electrochemical Soc. 81, 485 (1942).

13. B. L. Cross & N. Hackerman, Corrosion 10, 407 (1954).

14. E. J. Simmons, Corrosion 11, 255t (1955).

15. A. Hickling and F. W. Salt, Trans. Faraday Soc. 33, 1540 (1937).

16. A. J. Ferguson, Trans. Electrochemical Soc. 76, 113 (1939).

17. S. Schuldiner and R. E. White, J. Electrochemical Soc. 97, 433 (1950).

18. D. Stalropoulos, E. Yeager, and F. Hovorka, ibid, 98, 68 (1951).

19. H. Fischer, M. Seipt, and G. Morlock, Proc. 6th Meeting International Comm. for Electrochemical Thermo. (London, 1955), p. 239.

20. V. Bertocci, et. al., Ann. Chim. (Rome) 44, 44 (1954).

21. D. Reichenstein, Z. Electrochem. 15, 913 (1909).

22. D. F. Wohr, ibid, 39, 756 (1933).

23. M. Shaw and A. F. Remick, J. Electrochemical Soc. 97, 324; 335 (1950).

24. W. E. Haupin, ibid, 103, 174 (1956).

25. A. Dravnieks and H. A. Cataldi, Corrosion 10, 224 (1954).

26. G. A. Marsh and E. Schashl, Oil and Gas J. 54, No. 29, 125 (1955).

27. H. C. Gatos, Corrosion 12, 322t (1956).

28. M. Stern, J. Electrochemical Soc. 102, 609 (1955).

29. M. Stern and A. L. Geary, ibid, 104, 56 (1957).

30. M. Stern, ibid, 104, 9 (1957).

31. M. Stern, ibid, 104, 500 (1957).

32. M. Stern, ibid, 104, 645 (1957)

33. M. Stern, Corrosion 14, 329t (1958).

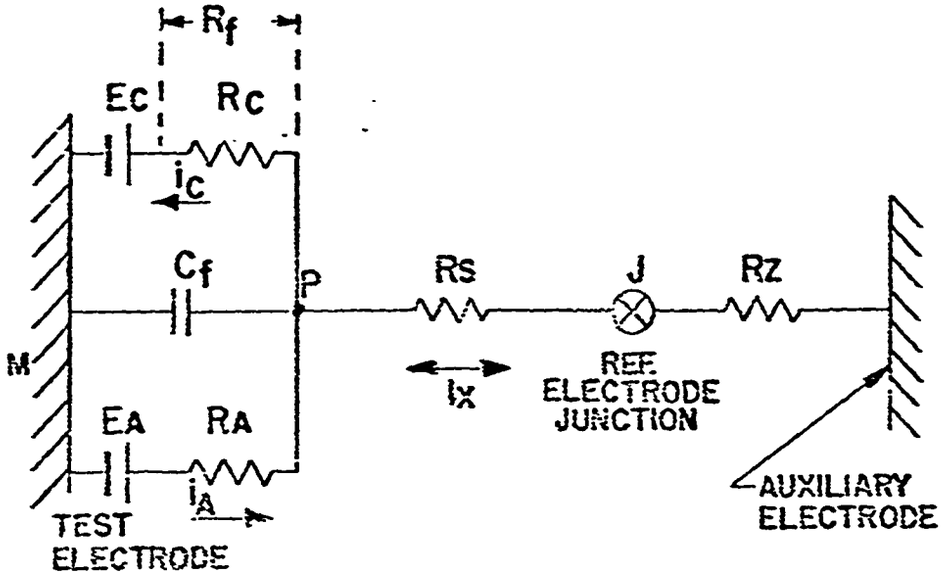

FIGURE 1. EQUIVALENT CIRCUIT OF POLARIZATION CELL

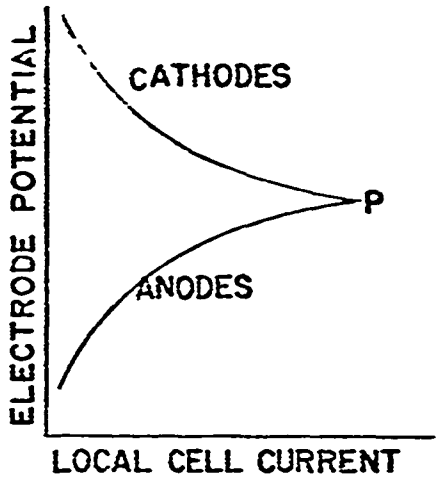

FIGURE 2. GENERALIZED LOCAL CELL POLARIZATION DIAGRAM

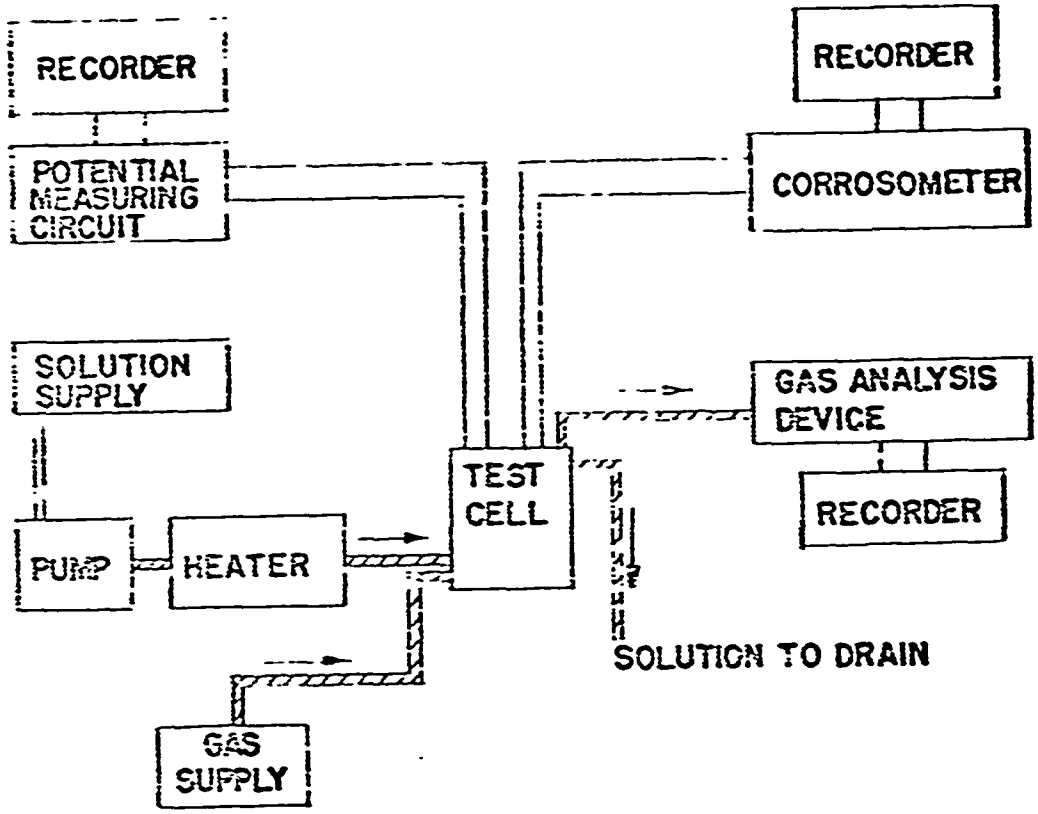

FIGURE 3. BLOCK DIAGRAM OF OVERALL TEST SYSTEM

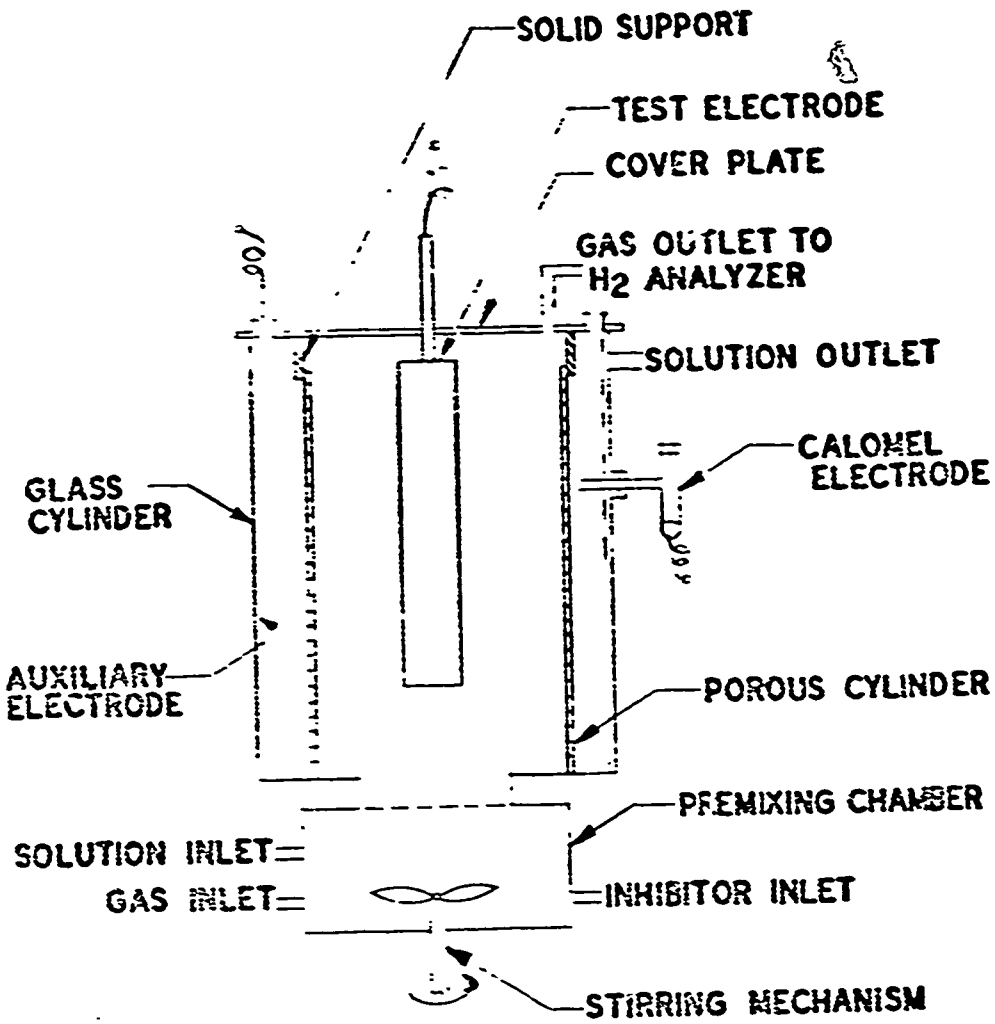

FIGURE 4. CONCENTRIC TYPE TEST CELL

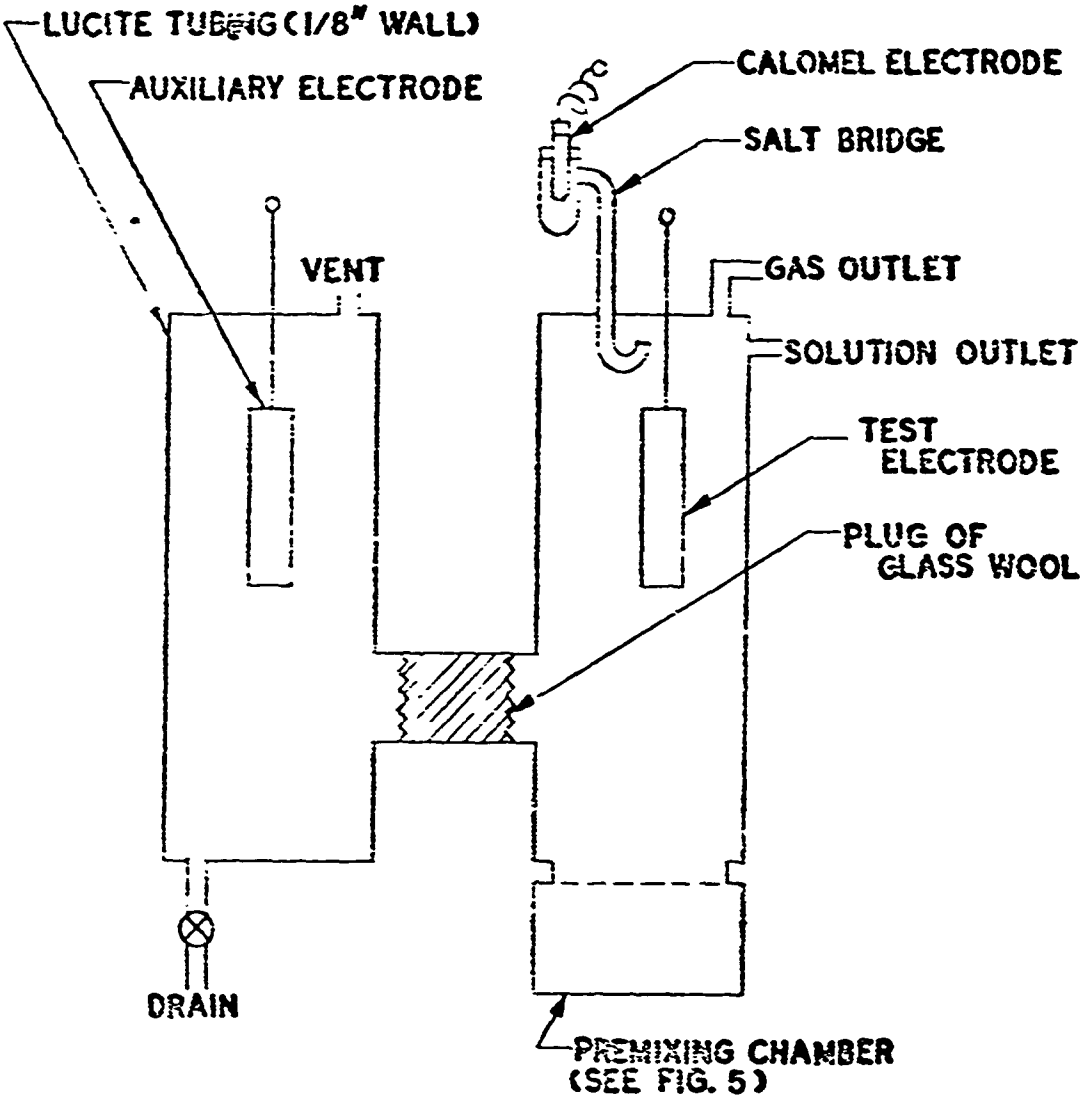

FIGURE 5. H-TYPE TEST CELL

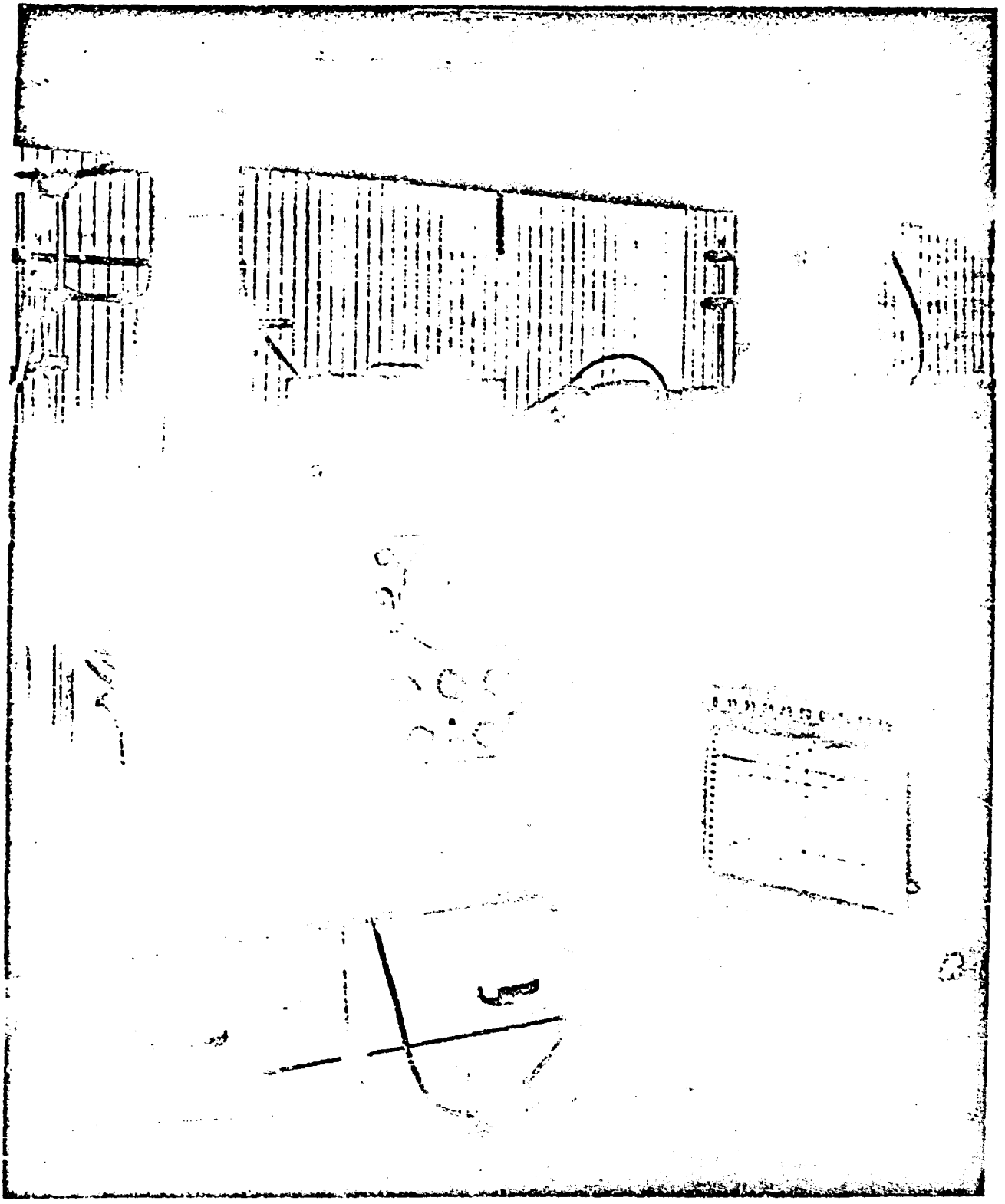

FIGURE 6. PHOTOGRAPH OF TEST SETUP

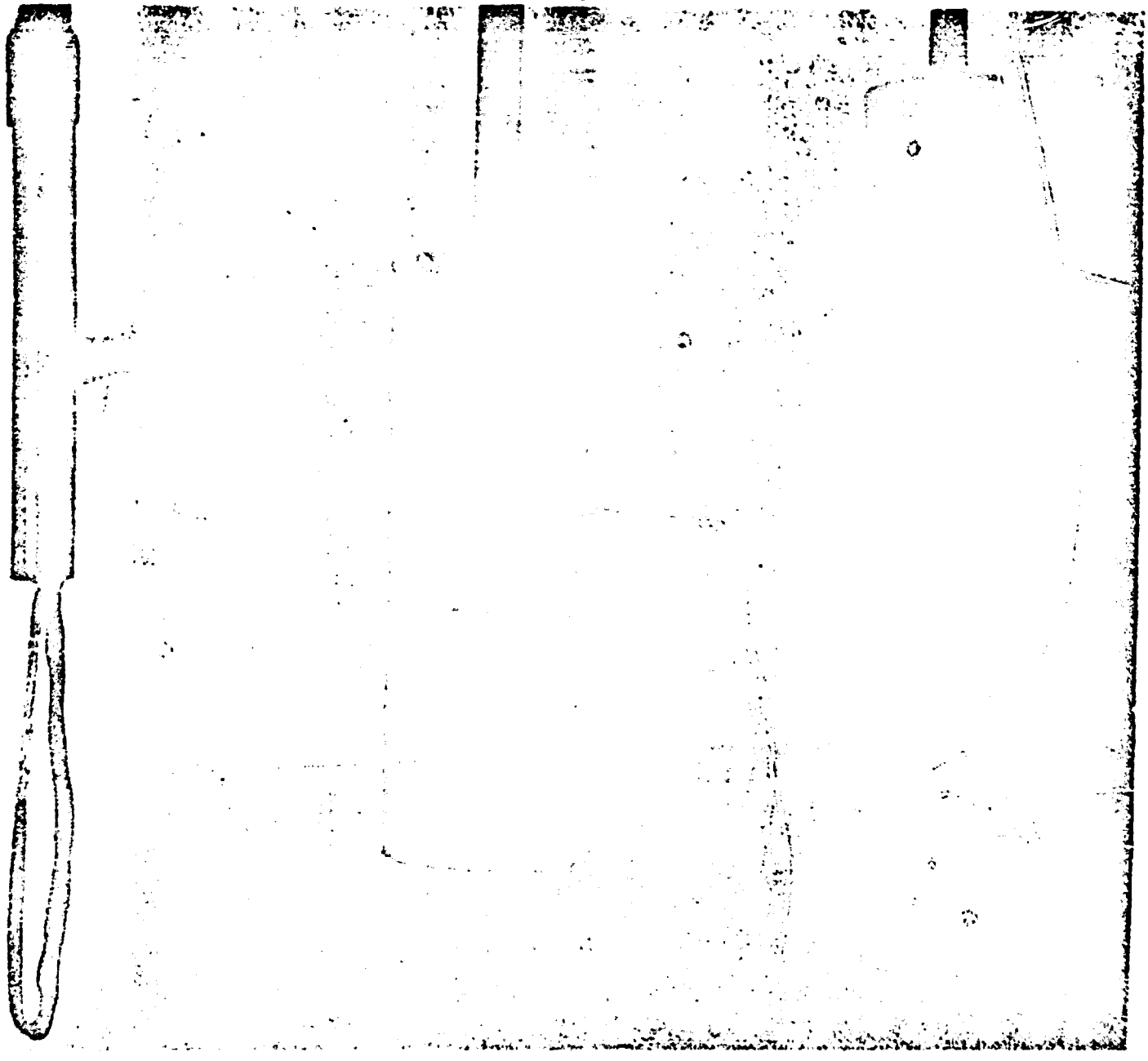

FIGURE 6A. PHOTOGRAPH OF TEST PROBES
Left: Standard Probe Center: Spiral Probe Right: Tubing Section

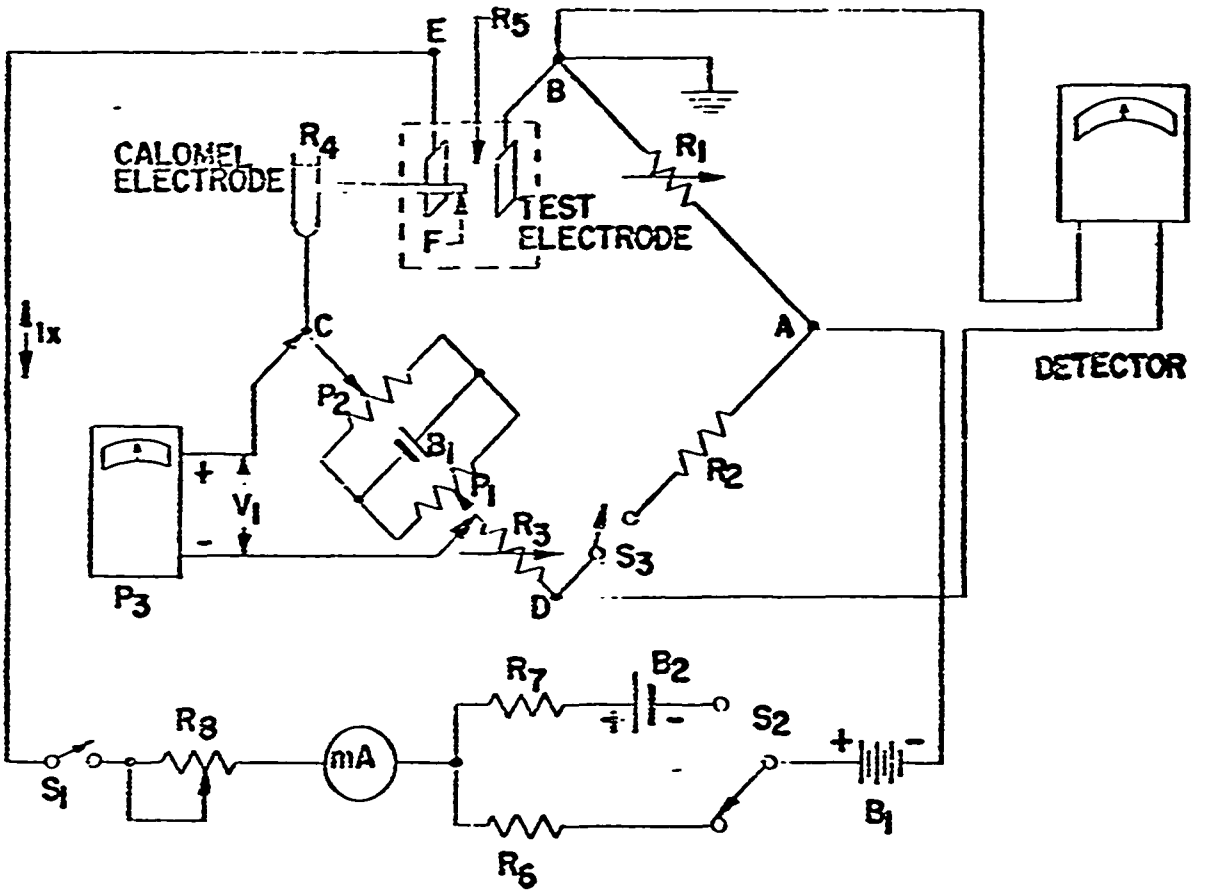

FIGURE 7. SCHEMATIC DIAGRAM OF PEARSON-HOLLER BRIDGE CIRCUIT

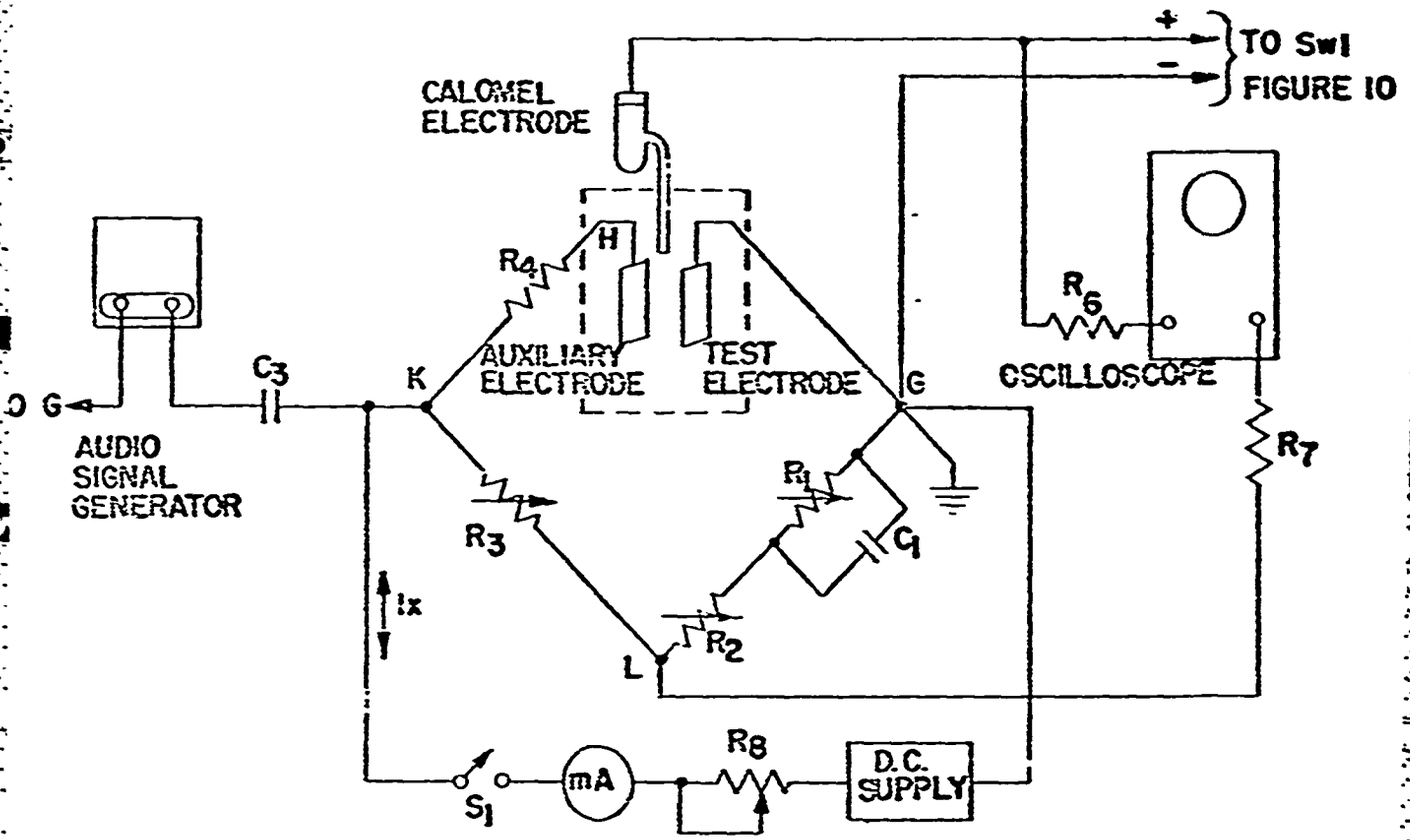

FIGURE 6. SCHEMATIC DIAGRAM OF D. C. - A. C. IMPEDANCE BRIDGE

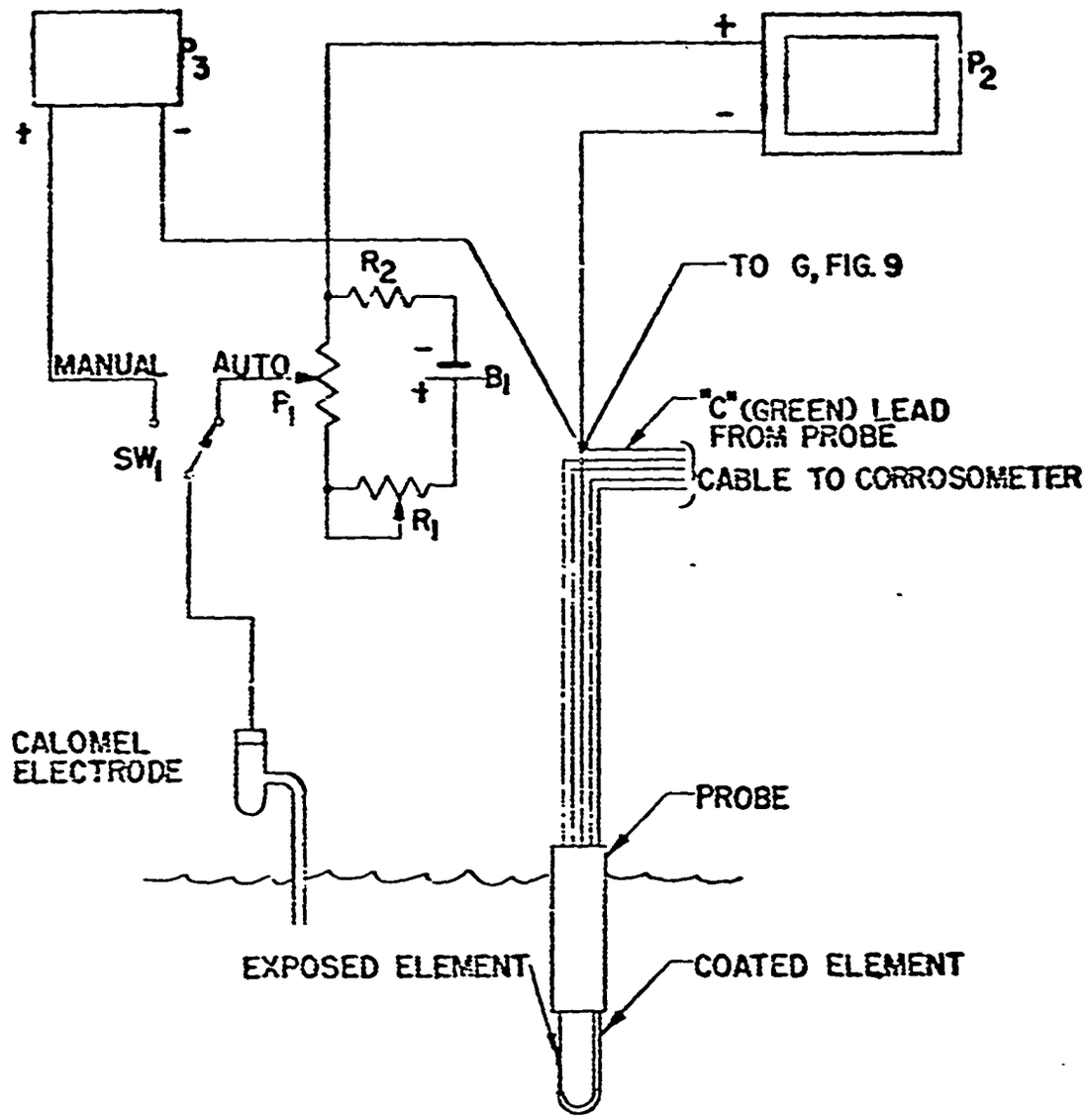

FIGURE 9. DETAIL OF ELECTRICAL CONNECTIONS USED FOR POTENTIAL MEASUREMENTS

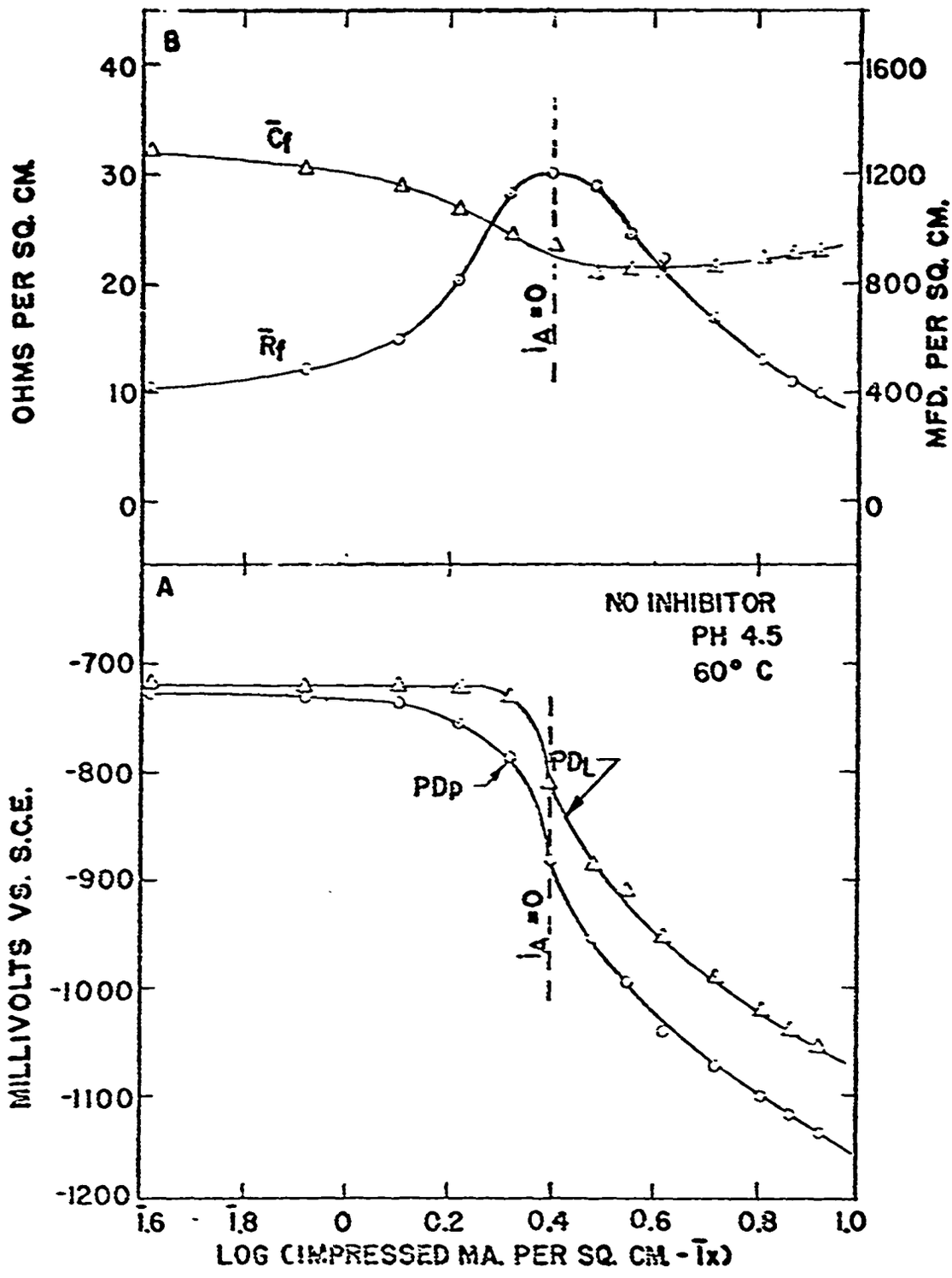

FIGURE 10. CATHODIC POLARIZATION OF UNINHIBITED ELECTRODE BY INTERMITTANT CURRENT

A. Potentials B. Interface Resistance and Capacitance

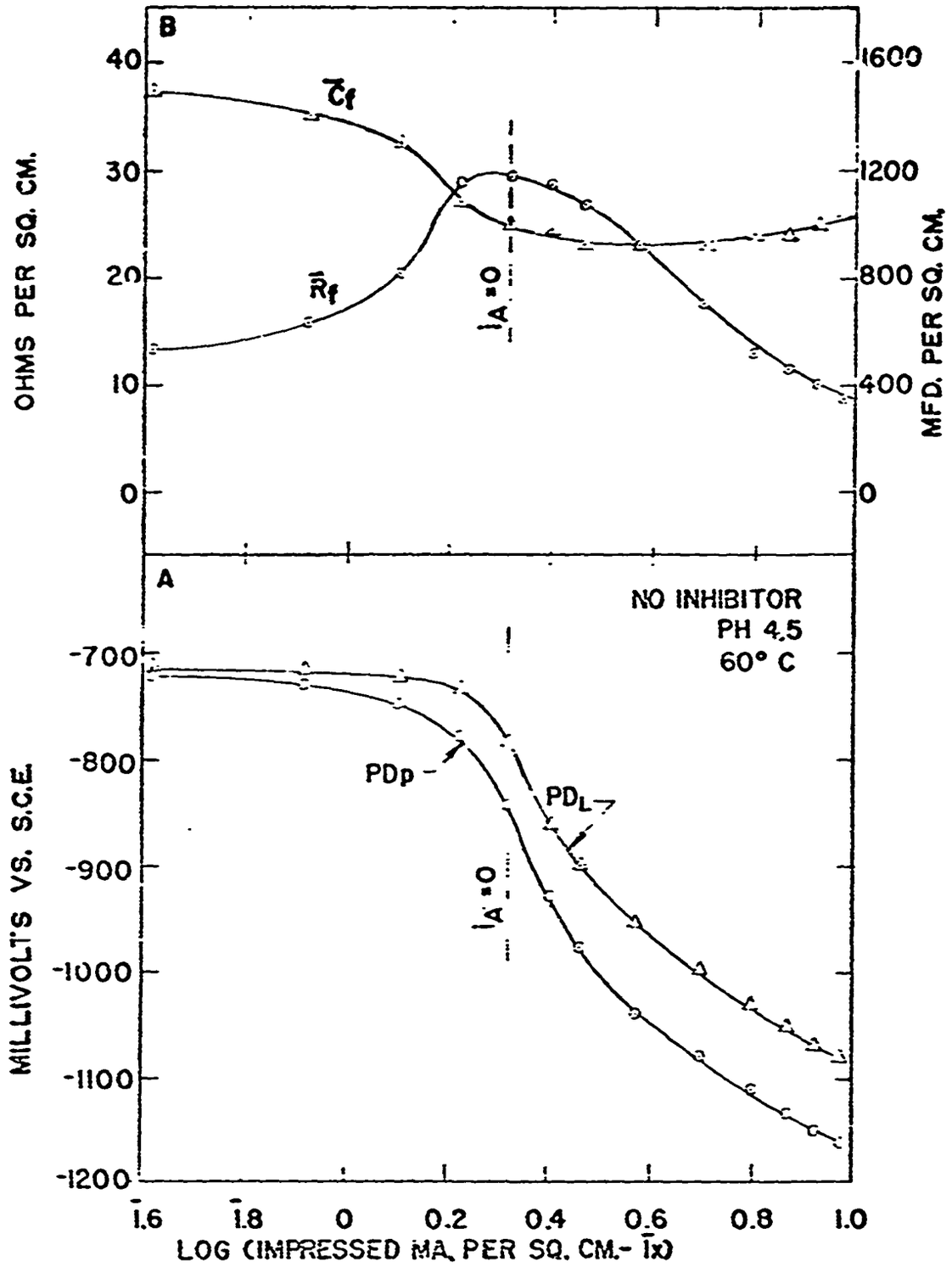

FIGURE 11. CATHODIC POLARIZATION OF UNINHIBITED ELECTRODE BY CONTINUOUS CURRENT

A: Potentials B: Interface Resistance and Capacitance

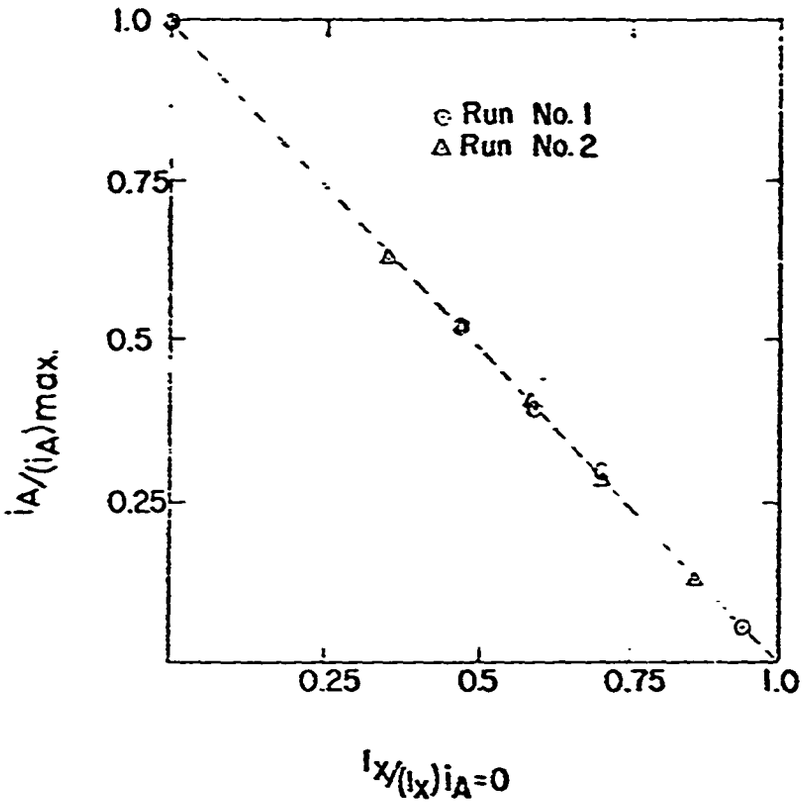

FIGURE 12. EMPERICAL PELATIONSHIP BETWEEN LOCAL ANODE CURRENT (i_A) AND IMPRESSED CURRENT (I_x)

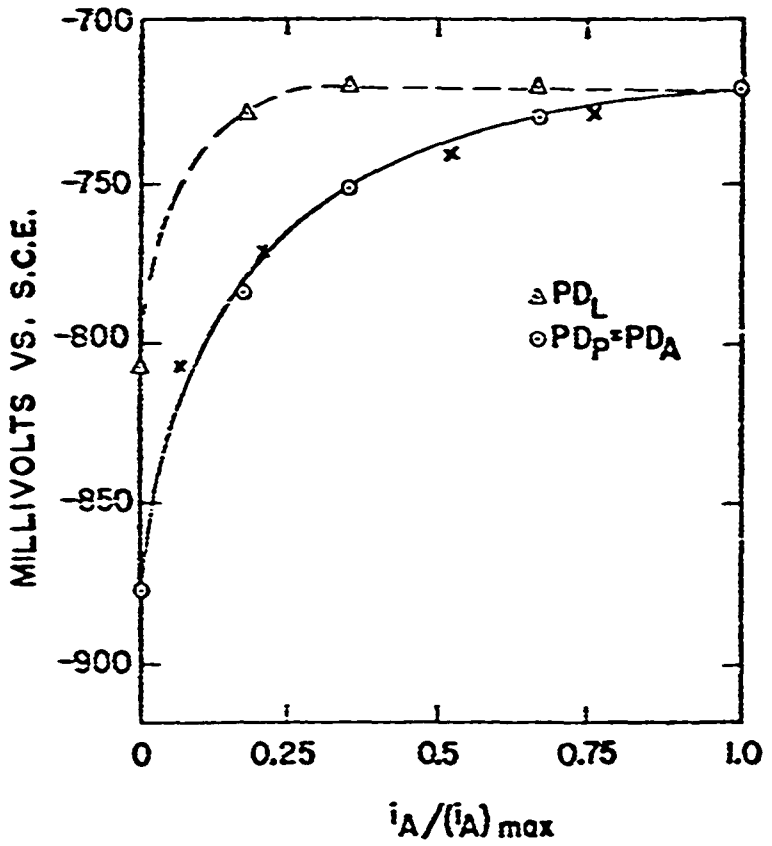

FIGURE 13. LOCAL ANODE POLARIZATION CURVES - UNINHIBITED ELECTRODE, INTERMITTANT CURRENT DATA

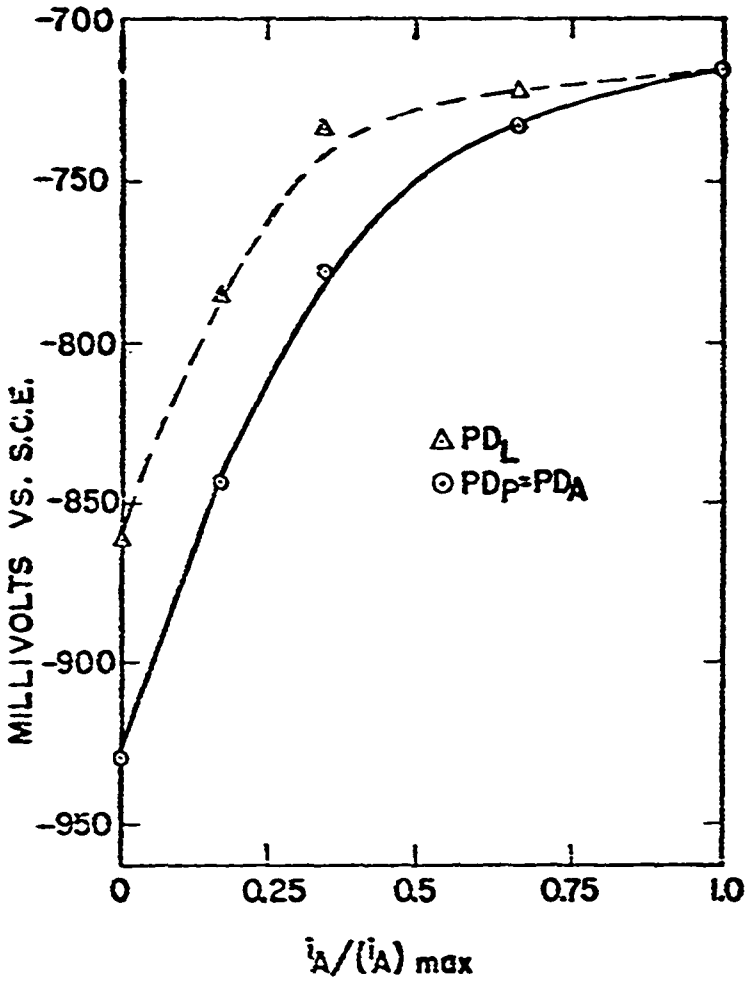

FIGURE 14. LOCAL ANODE POLARIZATION CURVES - UNINHIBITED ELECTRODE. CONTINUOUS CURRENT DATA

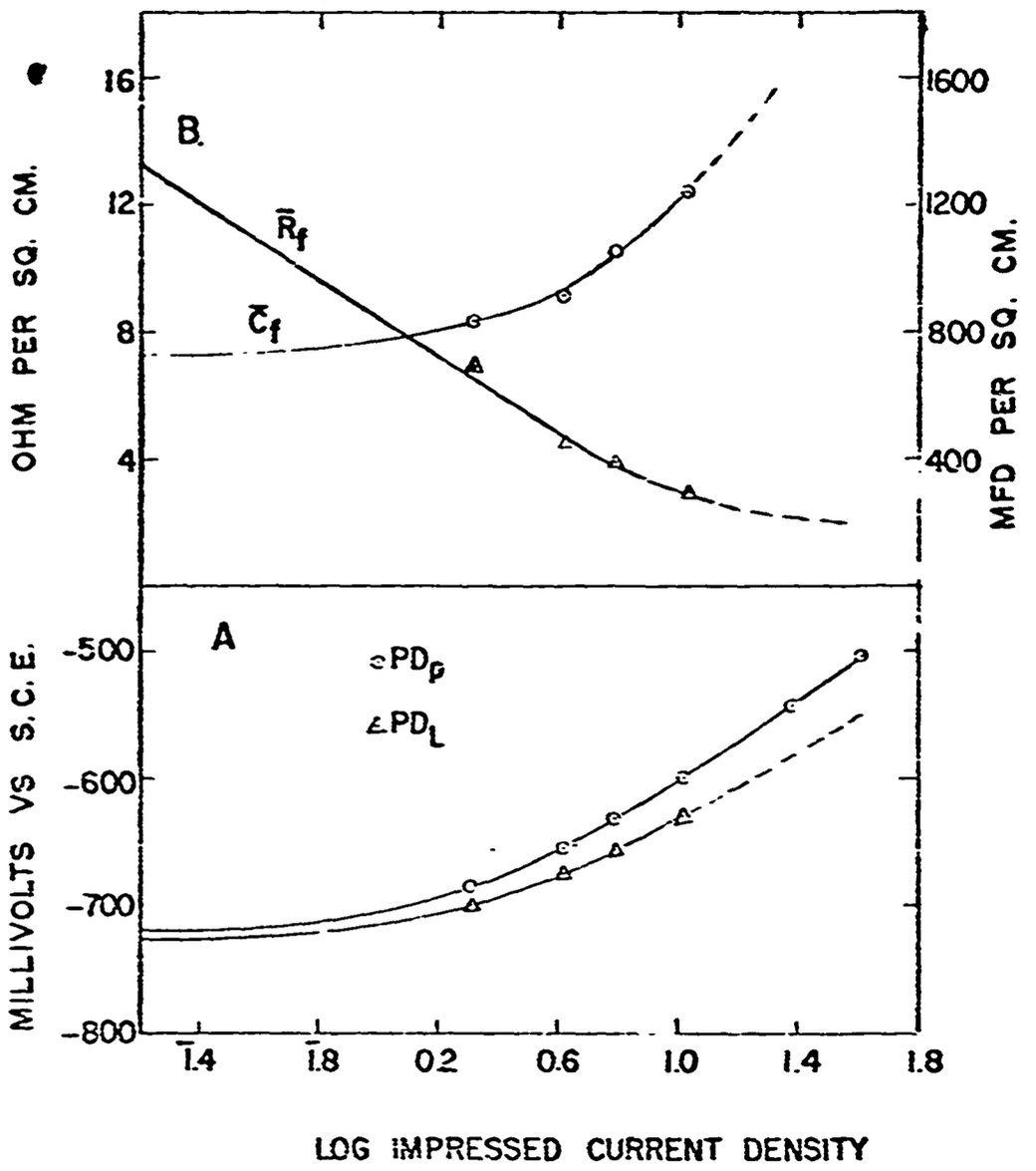

FIGURE 15. ANODIC POLARIZATION OF UNINHIBITED ELECTRODE

A: Potentials B: Interface Resistance and Capacitance

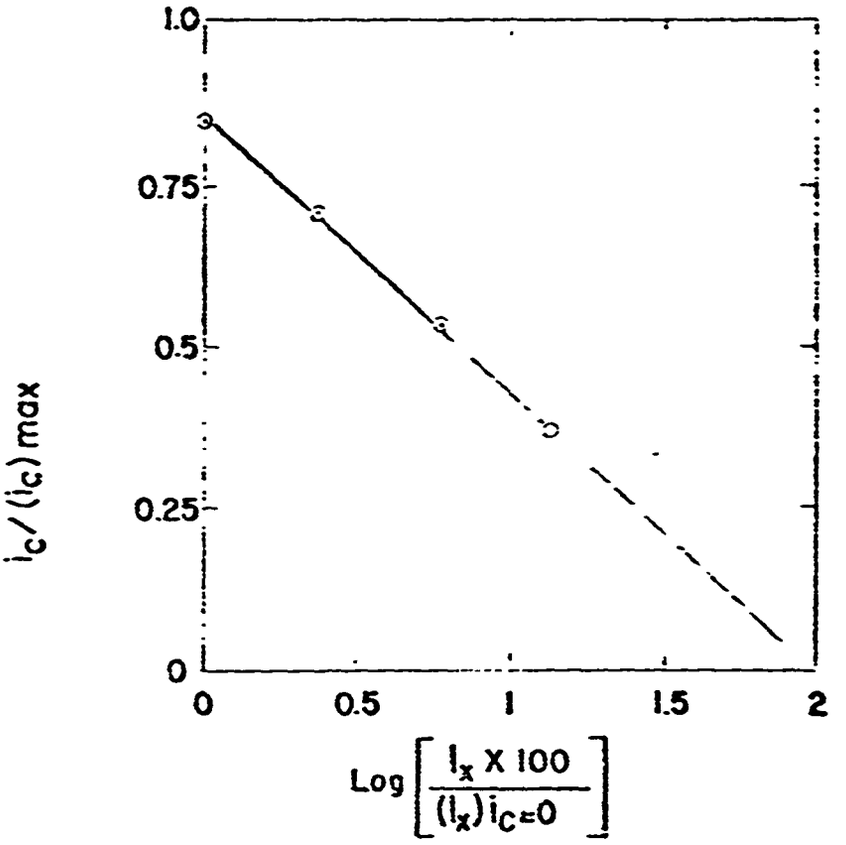

FIGURE 16. EMPERICAL RELATIONSHIP BETWEEN LOCAL CATHODE CURRENT (i_C) AND IMPRESSED CURRENT (I_x)

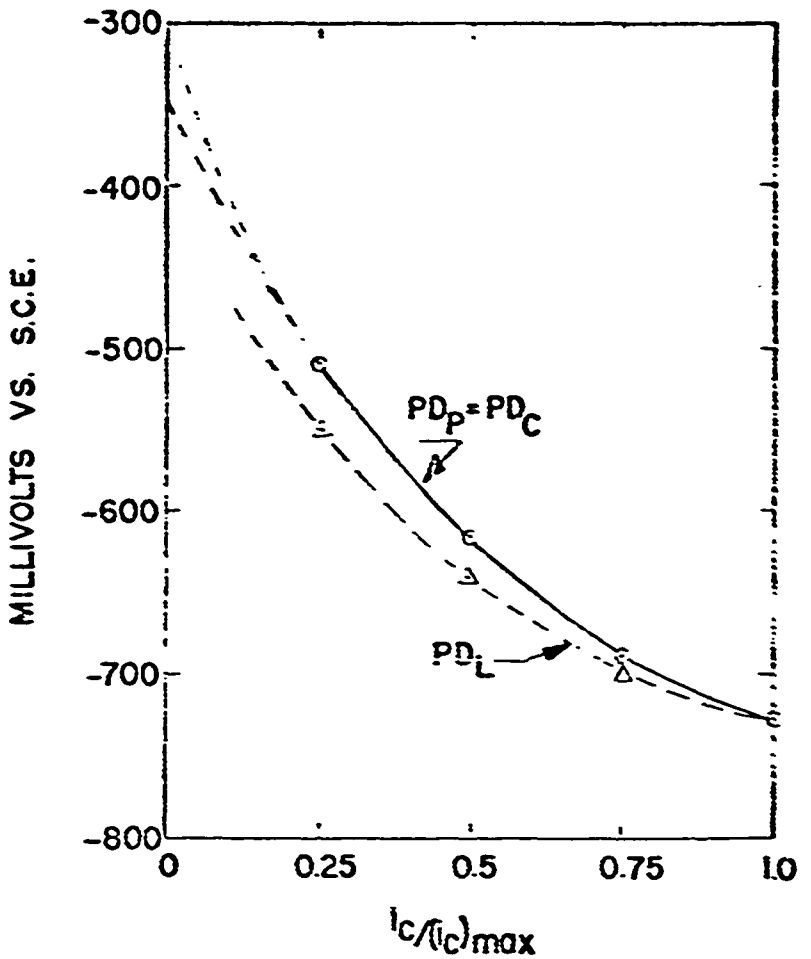

FIGURE 17. LOCAL CATHODE POLARIZATION CURVES - UNINHIBITED ELECTRODE

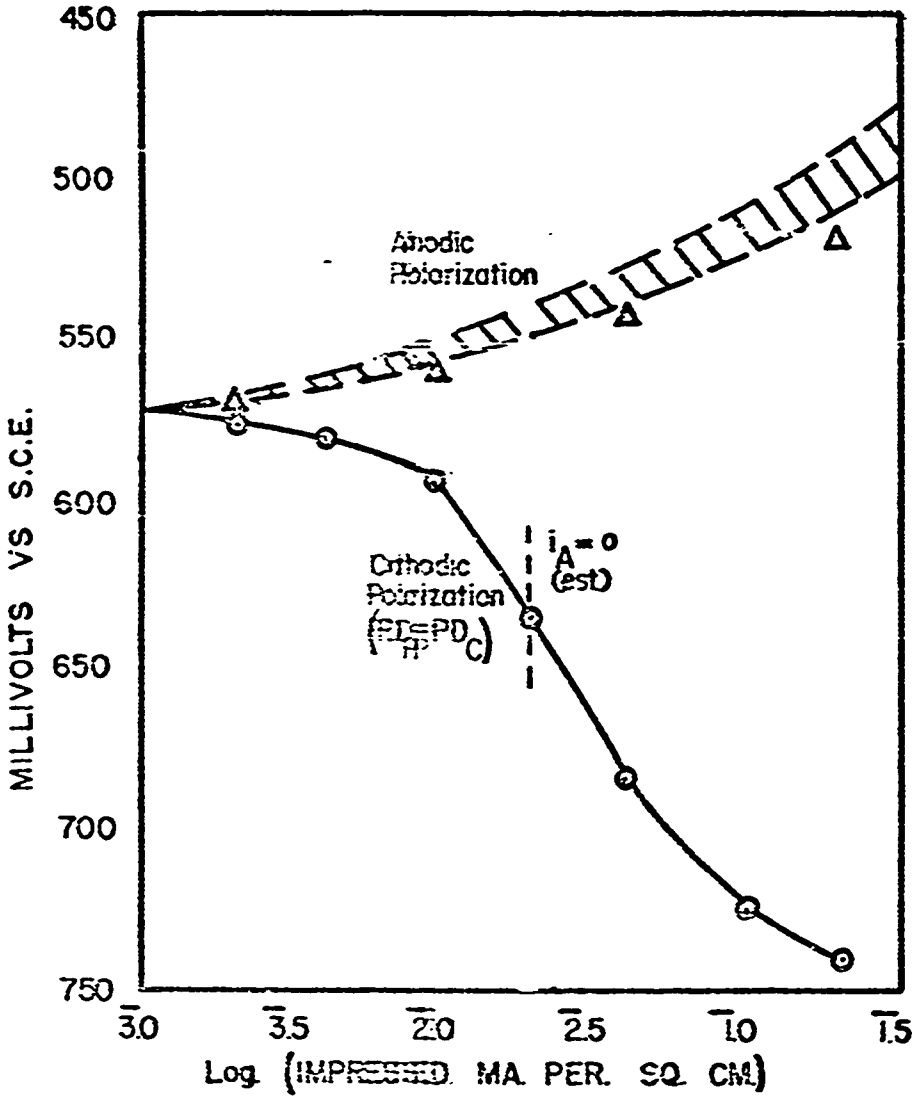

FIGURE 18. MIXED-POTENTIAL POLARIZATION CURVES FOR SODIUM ARSENITE AT 50 PPM.

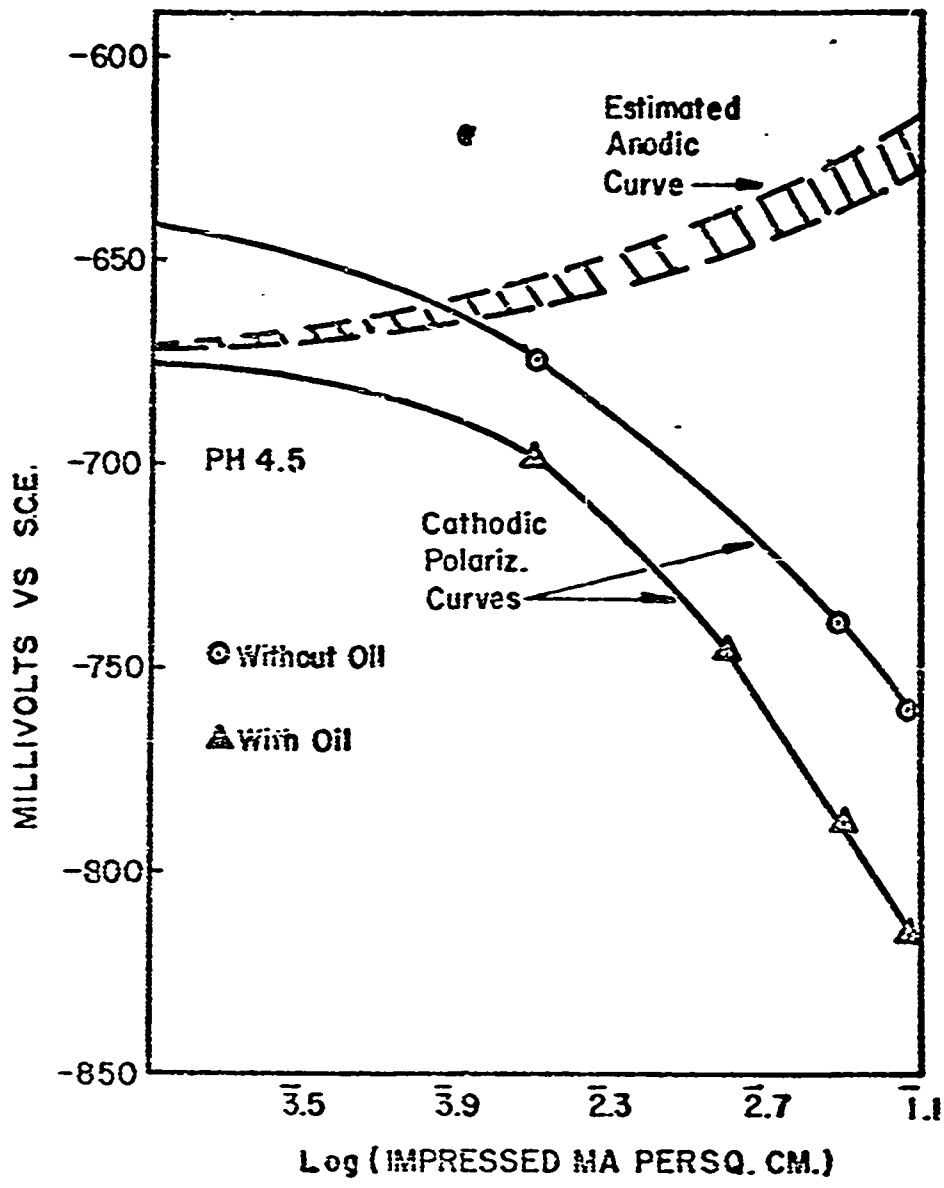

FIGURE 19. MIXED POTENTIAL POLARIZATION CURVES FOR A SUBSTITUTED IMIDAZOLINE (See Text)

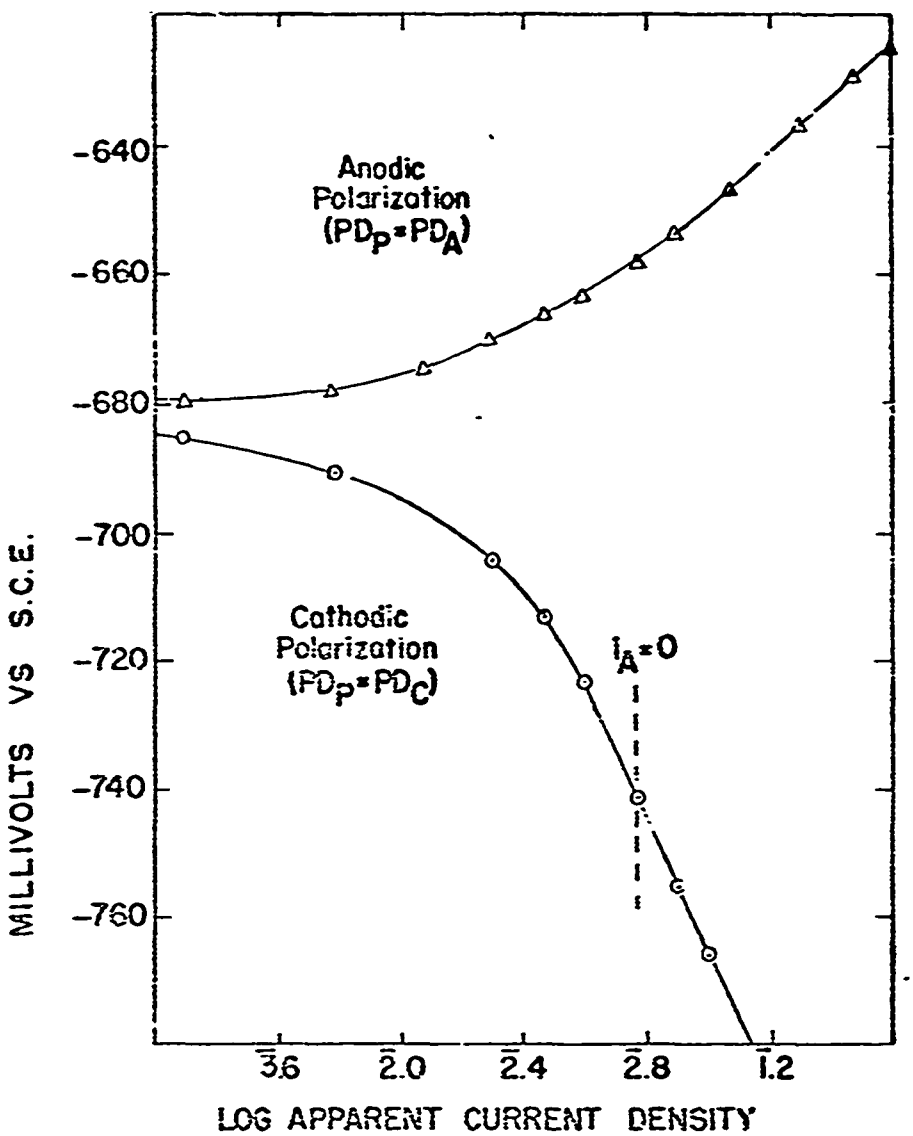

FIGURE 20. MIXED POTENTIAL POLARIZATION CURVES FOR A SUBSTITUTED THIOUREA (See Text)

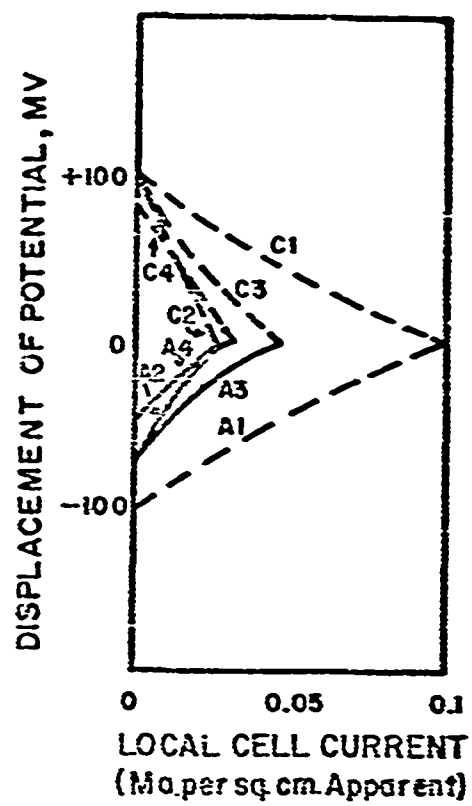

Curve 1. Sodium Ferrocyanide
Curve 2. Sodium Arsenite
Curve 3. Subst. Imidazoline
Curve 4. Thiourea Derivative

FIGURE 21. COMPOSITE LOCAL CELL POLARIZATION DIAGRAM FOR FOUR INHIBITORS

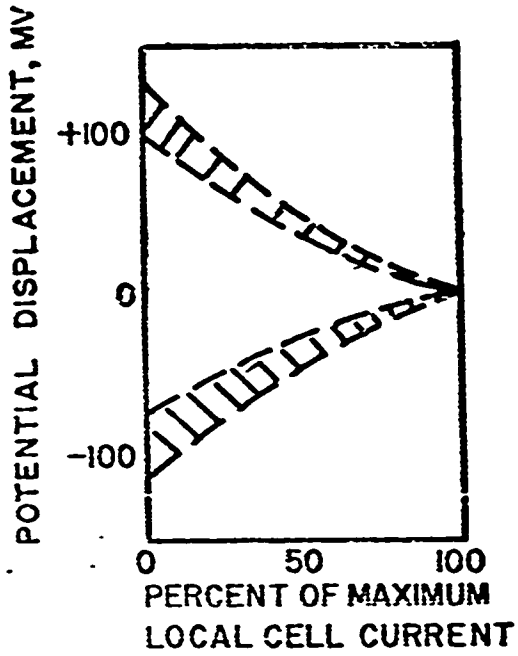

FIGURE 22. LOCAL CELL POLARIZATION DIAGRAM FOR SODIUM FERROCYANIDE AT 100 PPM.

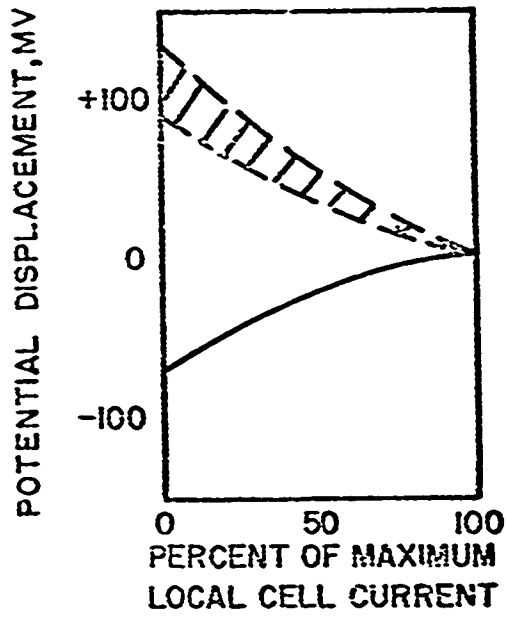

FIGURE 23. LOCAL CELL POLARIZATION DIAGRAM FOR SODIUM ARSENITE AT 50 PPM.

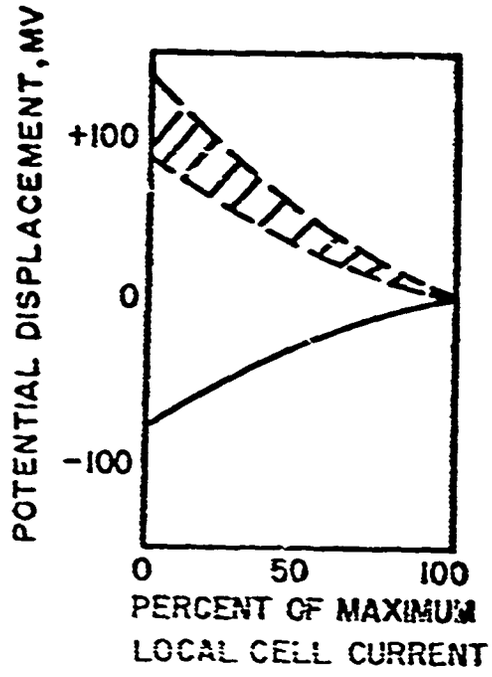

FIGURE 24. LOCAL CELL POLARIZATION DIAGRAM FOR A SUBSTITUTED IMIDAZOLINE AT 100 PPM.

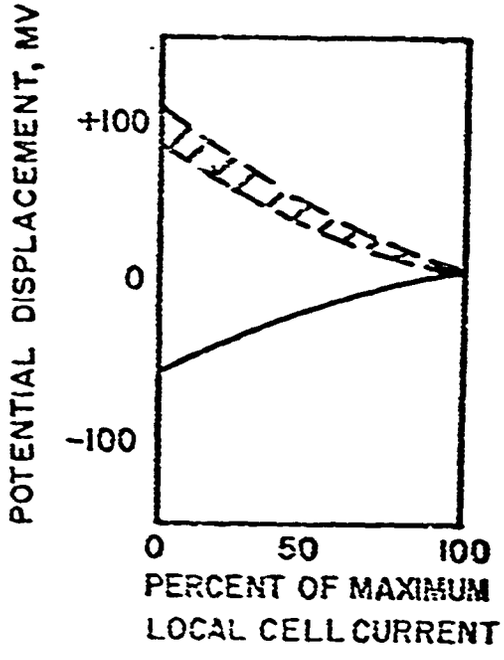

FIGURE 25. LOCAL CELL POLARIZATION DIAGRAM FOR A SUBSTITUTED THEOUREA AT 50 PPM.

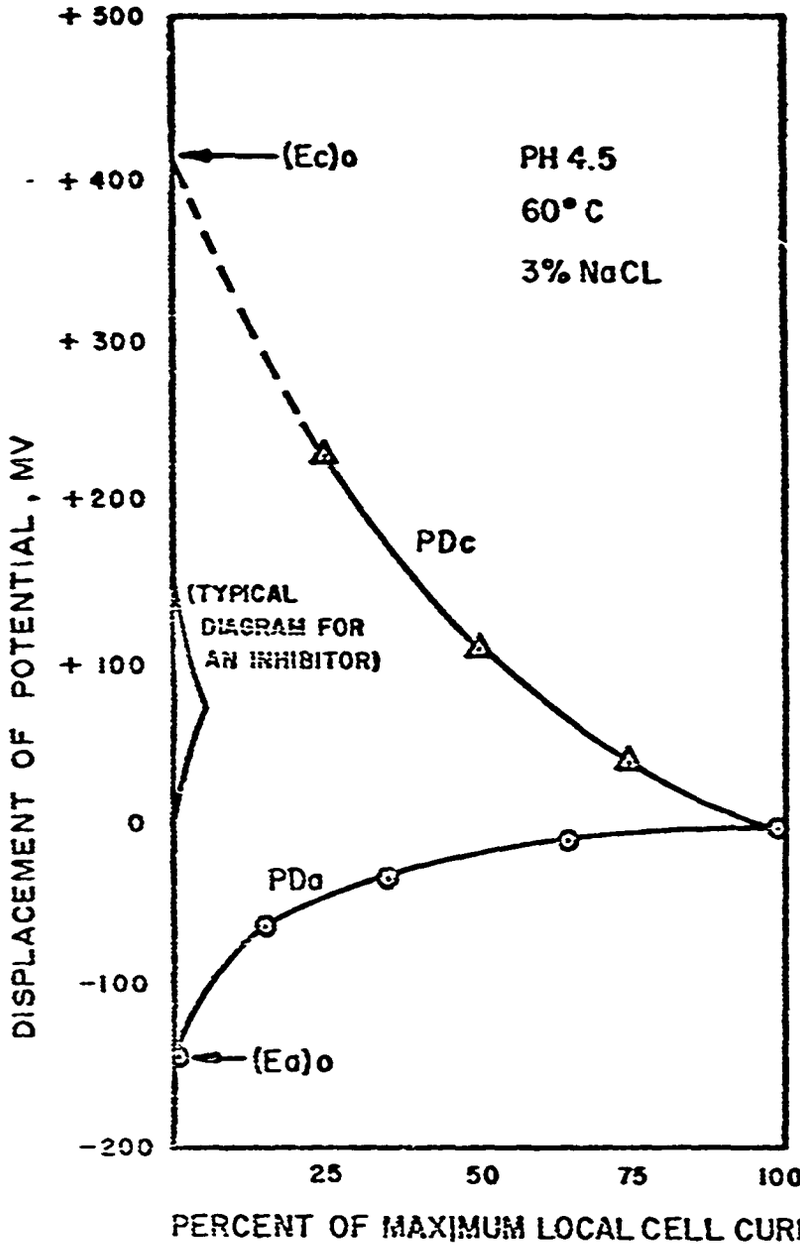

FIGURE 26. COMPLETE LOCAL CELL POLARIZATION DIAGRAM FOR THE UNINHIBITED ELECTRODE WITH A TYPICAL INHIBITOR DIAGRAM TO SCALE